UNIVERSIDAD AUTÓNOMA DE YUCATÁN

FACULTY OF ENGINEERING

POSTGRADUATE AND RESEARCH UNIT

THERMAL INVESTIGATION OF A PHOTOVOLTAIC AIR COLLECTOR INTEGRATED WITH A PHASE CHANGING MATERIAL

THESIS

PRESENTED BY:

RASIKH TARIQ

TO OBTAIN THE DEGREE OF:

MASTER'S IN ENGINEERING

OPTION: RENEWABLE ENERGY

MERIDA, YUCATAN, MEXICO

2020

ACKNOWLEDGMENT

First and foremost, all praises to the Almighty Allah who bestowed me the patience and strength throughout my life to continue the struggle to accomplish my goals.

I would like to offer my gratitude to Professor Bassam Ali for his counseling and guidance especially helping me to introduce the life-style in a country with a completely new language, and culture. It is fortunate for me to work with Professor J. Xamán and would like to appreciate his guidance and corporation, and especially for the time he spared for my research from his busy schedule. Nevertheless, it is the skillful expertise of Professor J. Xamán that this research ended up with a successful defense. I also owe thanks to my evaluation committee, Professor Ricalde, and Professor Mauricio, owing to their critical and positive discussion to improve this work. I would also acknowledge the administrative support of the current head of the postgraduate unit, Dr. Osvaldo Carvente Muñoz, and the previous head of the postgraduate unit, Dr. Carlos Quintal. I would also like to mention the gratitude of my colleagues and friends especially Dr. Adrian, Mario, Nicolas, Sandino, Francisco Aguilar, Ivan, Max, Francisco Pa, and Dr. Oscar.

This work is just not a result of my formation during the postgraduate degree, but also a result of my previous training experience. For this, I would like to offer thanks to Professor Sultan Khan to develop my theoretical formation in thermal engineering. The never-ending discussion with Professor Nadeem Ahmed Sheikh to generate new hypothesis and new knowledge which has always enlightened me. To Professor Changhong Zhan, for never giving up on my ideas, appreciating me, while maintaining a very deep relationship based on mutual trust. To my friend, Dr. Zahra Benarab, in all the amusing memories of the correction of my first article. These wonderful people are far in the space dimension, but I always carry their memories.

I would like to emphasize my love for my family for their continuous encouragement and appreciation. A special mention of my parents, who without a formal education, supported me to reach until here in my life.

This work is dedicated with love to my wife, Daniela Hernandez, for her compassion and unconditional support during all the ups and downs in our life as I certainly owe my success to her. I also dedicate this work to our child, Khalek Rasikh, who was with me even when I was struggling with my programming codes during midnight at 3 am, and I would just feel an immeasurable peacefulness and calmness even to my soul while hugging him.

Finally, I am thankful for the financial assistance granted by CONACYT (CVU no. 949314, scholarship no. 730315) to pursue a postgraduate degree in Universidad Autónoma de Yucatán, Mexico.

ABSTRACT

The integration of a PVT-air collector with phase changing material is subjected to local climatic dynamics. The prime novelty of this work is to include the climatic dynamics for PCM selection specifically for Mexico and analyzing the system based on multi-disciplinary parameters. In this work, yearly equivalent analysis is carried out for three different Mexican climatic zones within the Köppen classification (Aw, BSh, and Cwb) to select the optimal phase-changing material. Multi-disciplinary performance indicators are analyzed which are based on energy, exergy, exergetic sustainability, life cycle CO_2 emissions, enviroeconomic, exergoenvironmental, and economic analysis. The results have shown that a temperature decrement as high as ~20% can be attained for the best-selected phase-changing material. The electrical, thermal and exergetic efficiency ranges from ~8 to ~11%, 25 to ~33% and ~13 to ~17% respectively. The carbon pricing factor ranges from $20.00-$32.00 MXN per year. For the life cycle cost analysis, the local inflation, and the discount rate is considered. The Levelized Cost of energy ranges from $3.09 MXN/(kWh) to $4.30 MXN/(kWh) and the payback period ranges from ~10 to ~15 years.

RESUMEN

La integración de un colector de aire PVT con material de cambio de fase está sujeta a la dinámica climática local. La principal novedad de este trabajo es incluir la dinámica climática para la selección de PCM específicamente para México y analizar el sistema basado en parámetros multidisciplinarios. En este trabajo, se realiza un análisis equivalente anual para tres zonas climáticas mexicanas diferentes dentro de la clasificación de Köppen (Aw, BSh y Cwb) para seleccionar el material óptimo de cambio de fase. Se analizan los indicadores de desempeño multidisciplinarios que se basan en la energía, la exergía, la sostenibilidad exergética, las emisiones de CO_2 del ciclo de vida, el análisis ambiental, económico, ambiental y económico. Los resultados han demostrado que se puede lograr una disminución de la temperatura de hasta ~20% para el material de cambio de fase mejor seleccionado. La eficiencia eléctrica, térmica y exergética varía de ~8 a ~11%, 25 a ~33% y ~13 a ~17% respectivamente. El factor de fijación de precios del carbono varía de $20.00 a $32.00 MXN por año. Para el análisis del costo del ciclo de vida, se considera la inflación local y la tasa de descuento. El costo nivelado de energía varía de $3.09 MXN/(kWh) a $4.30 MXN/(kWh) y el período de recuperación varía de ~10 a ~15 años.

TABLE OF CONTENTS

LIST OF FIGURES

LIST OF TABLES

NOMENCLATURE

Abbreviations

CEP	Consumption of electrical power [W]
CRF	Capital recovery factor [-]
EPP	Electrical power production [W. m^{-2}]
LCC	Life cycle cost [MXN]
LCOE	Levelized cost of energy [MXN/(kW.h)]
NMEPP .	Net monthly electrical power production [kW. h]
MTHG	Monthly thermal heat generation [kW. h]
PWCC .	Present worth of capital cost [MXN]
TAC	Total annual cost [MXN]

Letters

a	Height of the channel [m]
A	Area [m^2]
AM	Air mass [-]
b	Width of the channel [m]
Br	Temperature coefficient of the PV module [K^{-1}]
c_p	Specific heat [J. kg^{-1}. K^{-1}]
$C_{extinction}$	Extinction coefficient [-]
D_h	Hydraulic diameter [m]
$\dot{Ex}$	Rate of exergy [W]
h	Heat transfer coefficient [W.m^{-2}. K^{-1}]
H_{latent}	Latent heat [J. kg^{-1}]
$i_{interest}$	Interest rate, [-]
$i_{inflation}$	Inflation rate, [-]
I	Incident Radiation [W.m^{-2}]
m	Mass flow rate [kg. s^{-1}]
M	Air mass modifier [-]
n	Day of the year [-]
Nu	Nusselt number [-]
RF_{index}	Reflective index [-]
S	Total absorbed solar radiation [W.m^{-2}]
t	Thickness [m]
$\tilde{t}$	Time, [s]
$t_{working}$	Working time [hours]

T .	Temperature, [K]
v_{wind}	Wind velocity [m. s^{-1}]
V	Volume [m^3]
x	x-dimension [m]
y	y-dimension [m]
z	z-dimension [m]

Symbols

ρ	Density [kg. m^{-3}]
η	Efficiency [%]
ϕ	Latitude angle [degrees]
δ	Earth's declination angle [degrees]
ω	Hour angle [degrees]
β	Title angle [degrees]
α	Absorptance [-]
κ	Thermal conductivity [$W.m^{-1}. K^{-1}$]
ε	Emissivity [-]
σ	Stefan-Boltzmann constant [$5.67x10^{-8}$ W. $m^{-2}. K^{-4}$]
$(\tau\alpha)$	Transmittance-absorptance [-]

Subscripts

amb	Ambient
b	Beam
conv	Convection
d	Diffused
ins	Insulation
in	Inlet
m	Melting
PV	Photovoltaic
rad	Radiation
ref	Reference
(s)	Solid
(l)	Liquid
(*eff*)	Effective
T	Total

CHAPTER 1. INTRODUCTION

The 2030 agenda of the United Nations (UN) (Santika et al., 2020) is a blueprint to achieve a sustainable future by addressing the global challenges in which ‘affordable and clean energy’ (Büyüközkan et al., 2018) has key importance. It focuses on the universal access to energy, increased energy efficiency (Bhadbhade et al., 2020), and the increased use of renewable energy making up sustainability (Piacentino et al., 2019) goal resilient to environmental issues like climate change. Each of the participating countries in this agenda has initiated goals to meet the UN 2030 target. In this regard, one of the goals of the Mexican 2030 agenda is to focus on affordable and non-polluting energy resources aligning with the global targets knowing the photovoltaic electricity generation potential in Mexico (see Fig. 1.1). However, it is quite challenging to meet such an enthusiastic goal without a proper regulation and support system in government policies. In this context, in December 2013, the Mexican Congress approved a series of constitutional amendments by allowing private investment in the national power sector of Mexico. These energy reforms boomed the solar energy sector particularly photovoltaic industry in Mexico since its implementation.

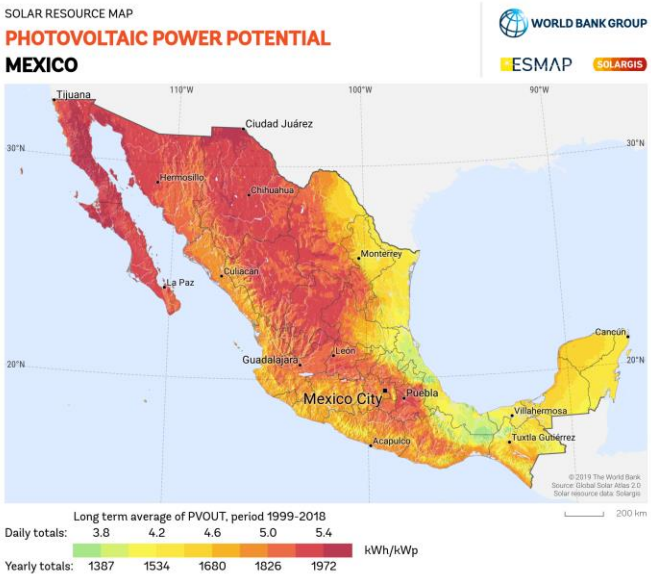

Fig. 1.1. Photovoltaic power potential in Mexico (ESMAP et al., 2019).

Photovoltaic (PV) (Singh et al., 2020) power generation plants, being a viable solar energy harvester, comes up with a unique set of technical problems primarily because of operational difficulties. These involve; sun being an intermittent energy resource and over-heating issue (Wajs et al., 2020). The excess PV heat is caused by the internal mechanism of the solid-state PV cells when some of the electrons of the higher frequency leave the conduction band on the incidence of solar energy. This phenomenon disrupts the reference temperature (25^{o}C) of the PV cells yielding a parameter called 'temperature coefficient' that produces a loss of power. The value of this coefficient for a typical monocrystalline solar cell is -0.45%. $^{o}C^{-1}$ indicating a photovoltaic efficiency loss of 0.45% per one degree increase in the operating temperature of PV panel (see Fig. 1.2). The operating temperature of the photovoltaic panel is a unique blend of many operational, geometric and climatic characteristics (Coskun et al., 2017). With this background, a photovoltaic panel must be installed with a local climatic feasibility study. Mexico: being a mega-diverse country in its climate, must go through a series of steps in its photovoltaic industry to meet the 2030 national and global sustainability agenda because the PV operating temperature can disorder the renewable energy mix in the national electricity grid.

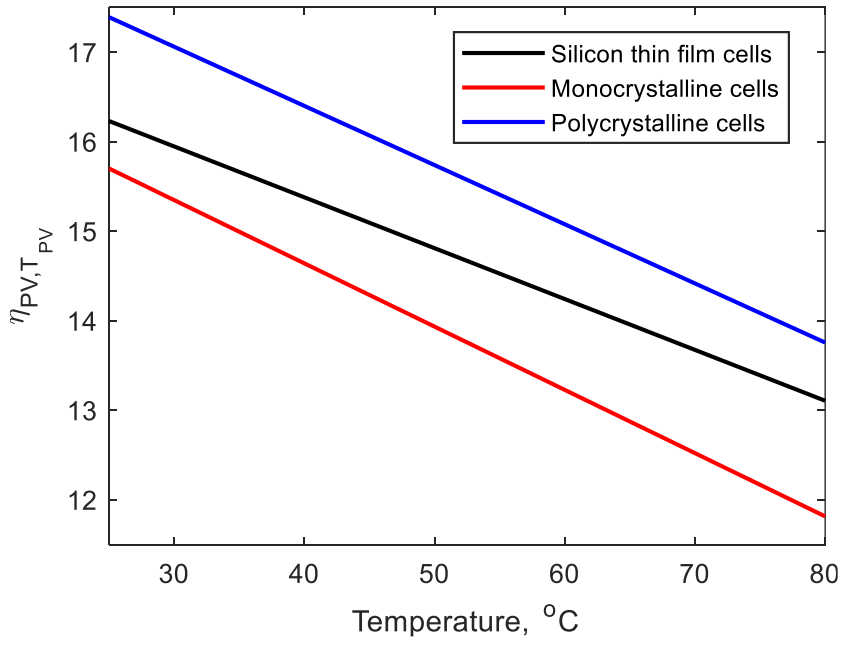

Fig. 1.2. Photovoltaic efficiency as a function of operating temperature for different technologies of solar cells.

1.1 Background Research

Several technical alternatives are available for the regulation of the operating temperature of the PV panel. The prime objective is the uniform cooling of the PV panel which can be attained by modern techniques like microchannels (Diallo et al., 2019), improved design of heat exchanger, heat pipes (Ren et al., 2020), jet impingement (K. M. Kim et al., 2014), combined microchannel-jet impingement, heat sinks and spreaders, dielectric cooling by direct immersion and making use of phase-changing materials (Nižetić et al., 2018). Each of the cooling methods is evaluated based on operating range, required energy consumption, investment, the requirement of turbomachinery, dependence on wind speed and direction, easiness of integration with PV module, heat rejection rate, and its maintenance. It can be concluded that the thermal management of photovoltaic panels with the use of phase-changing material (PCM) is a viable option. These PCM materials receive the excess heat of the photovoltaic panel and store it in the phase-changing process. However, PCM once charged; in terms of thermal heat, emits it back to the assembly. Furthermore, the excess heat during all the process can be used to satisfy the thermal energy demand of a residential or an industrial sector by heating a working fluid. Such a kind of assembly is called photovoltaic-thermal-collector (PVT) with a phase-changing material. (Preet et al., 2017) reported that the temperature of the PV module without any cooling technology is higher than the ambient temperature throughout the day and reaching as high as 85^{o}C. It is also reported that the temperature reduction is 47% and 53% by making use of PVT and PVT-PCM configurations.

The diverse nature of research on PVT-PCM is carried out in which (Al-Waeli, Chaichan, et al., 2019) analyzed a PVT system using nanofluid cooling and nano-PCM and reported an overall efficiency of 85.7%. (Sardarabadi et al., 2017) experimentally investigated ZnO-water nanofluid and PCM in the PVT system has reported that utilizing nanofluid, instead of water, can improve the overall thermal efficiency by 5% and overall exergy efficiency by 23%. (Stropnik & Stritih, 2016) integrated a PV panel with a phase-changing material and reported that the electric power production for the proposed integration has increased by 7.3% in one year for the city of Ljubljana, Slovenia. (Arıcı et al., 2018) also proposed the PV panel with a phase-changing

material; however, they utilized a simplified numerical model for the optimization of the PCM. Their results have reported that the integration has reduced the PV operating temperature for a maximum of ~10^{o}C. (Qiu et al., 2015) theoretically investigated the energy performance of the microencapsulated phase changing material-based PVT collectors. (Hossain et al., 2018) analyzed a two-side serpentine flow-based PVT-PCM collector based on energy, exergy, and economic analysis. They reported that the maximum electrical efficiency of PV and PVT-PCM collector was ~10% and ~11% respectively. (Gaur et al., 2017) numerically studied the electrical and the thermal performance of a PVT collector using PCM OM37 for the winter and summer days in Lyon, France, and reported that during the night time the PCM acts as a heat source and can provide the hot water which can be utilized in the next morning. (Yazdanifard et al., 2016) investigated the performance of PVT-PCM collectors in the laminar and the turbulent flow regime of the working fluid.

1.2 Theoretical framework

All these researches have particularly focused to use an incompressible fluid (water and/or nanofluid) in the PVT-PCM assembly. Water: being a working fluid, can possess many cons to the assembly causing corrosion in the piping and its leakage can lead to the total system failure. Similarly, nanofluids are going through tremendous problems of particle stability, sedimentation, segregation, and clogging. Using the current technology, nanofluid in a PVT-PCM assembly can be realized only in a control lab setup; yet practically it possesses great challenges for an apparatus on a commercial or an industrial scale.

Another alternative is to use an incompressible fluid like air in a PVT-PCM assembly. Despite the poor thermophysical properties of air, the air-based systems are practically preferred for lesser use of materials, low operating cost than water-based systems, there is a diverse utilization of air in the industrial processes, and it is also a clean transport fluid.

In this aspect, (Su, Jia, Alva, et al., 2017) proposed two different configurations of PVT-air-collector having PCM installed either below the backplate or below the air channel. Their results have concluded that the configuration having a PCM below the airflow is

not feasible because it shows an unstable behavior of overall efficiency during the whole day. In contrast, the configuration having PCM material installed below the backplate; quite near to the PCM material, offers higher stability, energy production, and thermal heat gain. However, (Su, Jia, Alva, et al., 2017) have only focused on the analysis of one day to deduce the results. The work (Su, Jia, Alva, et al., 2017) considered a PCM material having a melting peak at 28oC which can lead to the non-favorable PCM operational hours under dynamic performance. (Su, Jia, Alva, et al., 2017) consider the climatic data conditions of Nanjing, China which is humid subtropical (Cfa) (Pidwinry, 2011) climatic region, and the applicability of this configuration for other climatic regions is still dubious. Moreover, the work presented no details on the selection of a PCM material for these configurations.

Therefore, in this work, the prime novelty is to utilize the best configuration of (Su, Jia, Alva, et al., 2017) by identifying the gaps and enhancing the analysis using advanced thermodynamic analysis including exergy, entropy, environmental, economic, enviroeconomic, exergoenvironmental and exergoenviroeconomic analysis. Another novelty of this work is to focus on the Mexican climatic conditions to contribute towards the 2030 national agenda. Finally, one of the major contributions of this research towards the existing repository of this area is to provide a methodology systematically on the selection of PCM material for Mexican climatic conditions.

It is an on-going debate on the optimal PCM selection depending on the weather conditions. In this aspect, (Ma et al., 2018) presented a detailed mathematical model of a PV panel along with its sensitivity analysis. Their results reported that the two-dimensional analysis demonstrates that the peak temperature increases to about 5^{o}C for every 100 W.m^{-2} increase in the solar radiation, and the optimal performance of the PCM can be attained when its melting point is slightly higher (about 5^{o}C) than the ambient temperature. (Smith et al., 2014) provide a global insight into the energy generated by the photovoltaic panel considering the climatic data. They evaluated that the annual PV energy output is increased by ~6% for regions in Mexico and eastern Africa by using the optimal PCM melting temperature. They also reported that year-around dynamic climatic behavior might lead to durations when the optimal PCM melting temperature might not meet; however, the sub-optimal melting temperature still

produces an enhanced energy output. (Zhao et al., 2019) presented a year-around performance analysis of the PV with PCM and analyzed five PCM material of various melting ranges and the results indicate that those systems perform diversely under different weather conditions and seasons. They suggested that the PCM with a high melting temperature range usually performs well in summer but hinders heat transfer in winter since it will not be melted in the cold days which can lead to higher PV temperature. For a PCM having a low melting temperature range, it can perform better in winter, but it will be easily melted in the summer. Therefore, the study suggested using the PCM20 system for optimal performance.

Likewise, little research is carried on the climatic applicability of the PVT-PCM collectors. One such work is carried out on a PV-PCM configuration by (Khanna et al., 2018a). However, this analysis is not considered based on climatic classification (i.e. Köppen climate classification) nor it is for a PVT collector integrated with a phase-changing material. Their results have reported that the climatic regions having lower temperature fluctuations are suitable for the PCM integration, the heat extraction from the PV panel is more productive in a warm climate as compared to a cold climate, low wind-speeds are favorable for PCM integration, and climatic regions having higher solar insolation is also more productive for PCM.

Based on the established literature gap (refer to Table 1.1), it is identified that PVT-air-collector with PCM is hardly analyzed for weather conditions based on the advanced thermodynamic analysis. Additionally, no research of this kind is considered for the local climatic conditions of Mexico. Therefore, in this work, the authors have analyzed a PVT-air-collector with PCM for the Mexican climatic conditions. The system configuration is presented in Fig. 1.3 which is the most suitable as presented by (Su, Jia, Alva, et al., 2017). The photovoltaic panel is attached at the top of this assembly, followed by an aluminum backplate, a phase changing material, air channel, and insulation. A physical model based on energy analysis is established to deduce the system performance in terms of thermal heat gain, electricity power production, and overall efficiency. The prime objective of the work is to identify the most viable (in terms of thermal, economic and environmental performance) PCM material and quantity for the three climatic conditions of Mexico i.e. Savana (Aw), semi-arid (BSh) and highland

(Cwb) climates (Pidwinry, 2011). The work is enhanced by the usage of enviroeconomic, exergoenvironmental, and exergoenviroeconomic analysis.

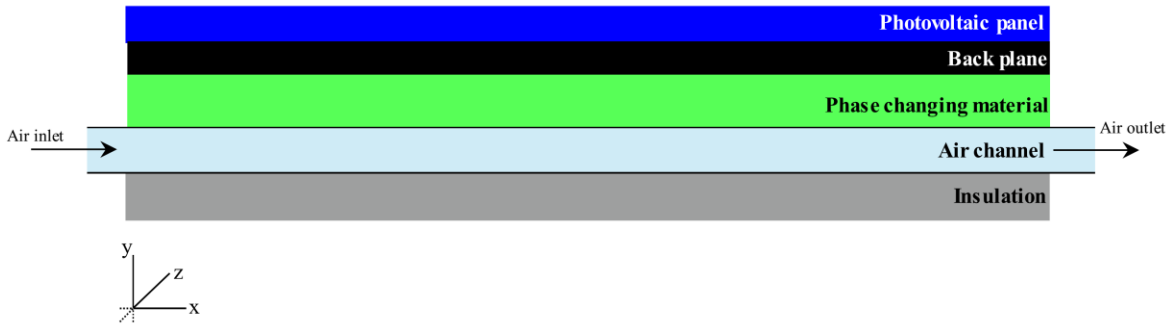

Fig. 1.3. Schematic diagram of the PVT air collector with PCM.

1.3 Hypothesis

The selection of a phase-changing material is dependent on local climatic conditions and the optimal phase-changing material can have viable thermodynamic performance indicators.

1.4 General objective

To apply the advanced thermodynamic tools assisted with a heat transfer analysis for an efficient, economical, and environmental-friendly photovoltaic thermal management with the usage of phase-changing material.

1.4.1 Specific objectives

1. To develop a mathematical model of the photovoltaic-thermal air collector integrated with a phase-changing material.
2. To resolve the governing mathematical model with an appropriate numerical model.
3. To select the best phase-changing material given the climatic conditions in Mexico.
4. To carry out a yearly analysis to evaluate the thermal performance for the most suitable phase changing material for each dominant Mexican climatic zone.
5. To evaluate the economic feasibility of the PVT-PCM assembly.

Table 1.1. A literature review on PVT PCM technology.

Reference	Type of Collector	Type of analysis	Type of working fluid analyzed?	Type of phase-changing material analyzed?	Duration of analysis?	Location of experimentation/analysis?	Climatic zone?
(Preet et al., 2017)	PVT-PCM	Energy analysis	Water	Paraffin wax RT-30	One day	Beant College of engineering and technology, Gurdaspur, India	-
(Hossain et al., 2018)	PVT-PCM	Energy analysis, Exergy analysis, and Economic analysis.	Water	Lauric acid	One day	University of Malaya, 59990, Kuala Lumpur, Malaysia	-
(Malvi et al., 2011)	PVT-PCM	Energy analysis	Water	Paraffin wax	One day	University of Leeds, LS2 9JT, United Kingdom	-
(Modjinou et al., 2019)	PVT-PCM	Energy analysis	Water	Macro-encapsulated PCM	Two days (January 10, 2018 and April 09, 2018)	Hefei (latitude 31^{o}N; longitude 117^{o}E), China	-
(Gaur et al., 2017)	PVT-PCM	Energy analysis	Water	Bio OM37 PCM	Two days (February 20, and July 08)	Lyon, France	-
(Yuan et al., 2018)	PVT with macro-encapsulated PCM	Energy analysis	Water	Parameters are mentioned but its type is not mentioned.	Two days of December 2017 and January 2018.	Hefei (latitude 31^{o}N; longitude 117^{o}E), China	-
(Fayaz, Rahim, Hasanuzzaman, Rivai, et al., 2019)	PVT-PCM	Energy analysis	Water	Paraffin (commercial code A44-PCM)	24 hours	University of Malaya, 59990, Kuala Lumpur, Malaysia	-

(Hosseinzadeh et al., 2018)	PVT-PCM	Energy analysis, and Exergy analysis.	Water	Organic paraffin wax	Selected days in August and September	Ferdowsi University of Mashhad, Iran	-
(Kazemian et al., 2018)	PVT-PCM	Energy analysis, Exergy analysis, and Entropy analysis.	Water, ethylene glycol and their mixture	Paraffin wax	9:30 a.m. to 3:30 p.m. on selected days in August	Ferdowsi University of Mashhad, Mashhad, Iran	-
(Su, Jia, Lin, et al., 2017)	PVT-PCM	Energy analysis	Water	Paraffin wax (a reference to [17])	One day	Nanjing, China	-
(Khanna et al., 2018b)	PVT-PCM	Energy analysis	Water	RT 25 HC PCM	-	-	-
(Su, Jia, Alva, et al., 2017)	PVT-PCM	Energy analysis	Air	The parameters of the PCM are mentioned but its exact name is not mentioned.	08:00 to 17:00 hours	Nanjing, China	-
(Z. Li et al., 2019)	PVT-PCM	Energy analysis	Water	Paraffin wax	18th to 19th of July 2018.	Building roof in the campus of Shanghai Jiao Tong University, Shanghai, China (31°1′14″N, 121°26′11″E)	-
This work	PVT-air-collector with PCM	Energy analysis, Exergy analysis, Entropy generation rate, etc.	Air	Tested different PCM materials to find the most viable option.	Yearly equivalent analysis	Three different locations (Campeche, Monterrey, and Mexico City)	Three different climatic zones (Aw, BSh, and CWb)

CHAPTER 2. MODELING SETUP

The mathematical model of the PVT air collector integrated phase-changing material is developed based on several assumptions which are listed here:

1 The properties of the different materials of the collector are homogenous throughout its construction (Modjinou et al., 2019; Preet et al., 2017).
2 Thermophysical properties of air at any cross-sectional area remains the same; however, they vary with respect to its flowing direction depending upon its temperature (R. Tariq et al., 2018; Rasikh Tariq et al., 2019).
3 Solar radiation is equally distributed on the surface area of the photovoltaic panel (Preet et al., 2017; Rasikh Tariq, Sheikh, et al., 2018).
4 The temperature and thermophysical properties are constant within the boundary of control volume for the converged results.
5 Conduction is the dominant mode of heat transfer inside the PCM (Yuan et al., 2018).
6 The melting and freezing phenomena of the PCM is symmetric (Fayaz, Rahim, Hasanuzzaman, Rivai, et al., 2019).
7 There is no dust or other deposits on the top of the photovoltaic panel (Preet et al., 2017).

2.1 Physical model based on energy balance

The energy balance on the photovoltaic panel is given by:

$$\left(\rho_{PV}\delta V_{PV}\right)c_{p,PV}\frac{\partial T_{PV}}{\partial \tilde{t}}=\begin{bmatrix} S-h_{conv,PV-amb}\left(T_{PV}-T_{amb}\right)-h_{rad,PV-sky}\left(T_{PV}-T_{sky}\right) \\ -U_{PV-back\ plane}\left(T_{PV}-T_{back\ plane}\right)-EPP_{PV} \end{bmatrix}\delta z\delta x \qquad (2.1)$$

The convective heat loss coefficient from the PV panel to the ambient is given by $h_{conv,PV-amb}=5.8+3.7v_{wind}$ (McAdams, 1954). The radiative heat loss coefficient from the PV panel to the sky is given by: $h_{rad,PV-sky}=\varepsilon_{PV}\sigma\left[T_{PV}+T_{sky}\right]\left[T_{PV}^{2}+T_{sky}^{2}\right]$ with $T_{sky}=0.0375T_{amb}^{1.5}+0.32T_{amb}$ (Ma et al., 2018). The electrical power production is given

in terms of the temperature of the photovoltaic panel and the reference temperature for the design conditions. It is given as (Skoplaki & Palyvos, 2009; Wang et al., 2019):

$$EPP_{PV} = I_T \eta_{PV,ref}[1 - Br(T_{PV} - T_{ref})] \tag{2.2}$$

where, $\eta_{PV,ref}$ is the efficiency of the PV panel under the reference temperature T_{ref} which is 25°C and Br is the temperature coefficient of the PV module. These values $\eta_{PV,ref}$ and Br are often specified by the manufacturer; therefore, the term $\eta_{PV,ref}[1 - Br(T_{PV} - T_{ref})]$ corresponds to the efficiency of the photovoltaic panel for its operating temperature T_{PV}.

The energy balance on the backplate is given by:

$$\left(\rho_{back\ plane}\delta V_{back\ plane}\right)c_{p,back\ plane}\frac{\partial T_{back\ plane}}{\partial \tilde{t}} = \begin{bmatrix}\left(1-\alpha_{PV}\right)S + U_{PV-back\ plane}\left(T_{PV} - T_{back\ plane}\right)\\ -U_{back\ plane-PCM,1}\left(T_{back\ plane} - T_{PCM,1}\right)\end{bmatrix}\delta z \delta x \tag{2.3}$$

The effective heat capacity model is utilized for the analysis of the PCM which includes its evaluation of properties during the solid, mushy as well as liquid phase. This effective heat capacity can be calculated depending upon the phase; thus, given by (Jiménez-Xamán et al., 2019):

$$c_{p(eff),PCM} = \begin{cases} [\text{Solid phase}] & c_{p(s),PCM} & T_{PCM} < (T_{m,PCM} - \Delta T_{PCM}) \\ [\text{Mushy phase}] & \dfrac{c_{p(s),PCM} + c_{p(l),PCM}}{2} + \dfrac{H_{latent}}{2\Delta T_{PCM}} & (T_{m,PCM} - \Delta T_{PCM}) \le T_{PCM} \le (T_{m,PCM} + \Delta T_{PCM}) \\ [\text{Liquid phase}] & c_{p(l),PCM} & T_{PCM} > (T_{m,PCM} + \Delta T_{PCM}) \end{cases} \tag{2.4}$$

where $c_{p(eff),PCM}$ corresponds to the effective heat capacity either for solid, mushy, or liquid phase, and $T_{m,PCM}$ is the melting temperature of the PCM. Eq. (2.4) must only be applied after evaluating the temperature of the PCM which can be calculated by applying the energy balance on each layer. Following this, the first layer of the PCM has two types of conductive heat losses. The first one is a conductive heat loss from

the absorber plate to the first layer of the PCM. The second one is also a conductive heat loss from the first layer of PCM to the interface of PCM 1 and PCM 2. In this way, the energy balance is given by:

$$\left(\rho_{(eff)PCM,1}\delta V_{PCM,1}\right)c_{p(eff)PCM,1}\frac{\partial T_{PCM,1}}{\partial \tilde{t}}=\begin{bmatrix}U_{back\ plane-PCM,1}\left(T_{back\ plane}-T_{PCM,1}\right)\\-U_{PCM,1-PCM,2}\left(T_{PCM,1}-T_{PCM,2}\right)\end{bmatrix}\delta z\delta x \tag{2.5}$$

$$\left(\rho_{(eff)PCM,2}\delta V_{PCM,2}\right)c_{p(eff)PCM,2}\frac{\partial T_{PCM,2}}{\partial \tilde{t}}=\begin{bmatrix}U_{PCM,1-PCM,2}\left(T_{PCM,1}-T_{PCM,2}\right)\\-U_{PCM,2-PCM,3}\left(T_{PCM,2}-T_{PCM,3}\right)\end{bmatrix}\delta z\delta x \tag{2.6}$$

$$\left(\rho_{(eff)PCM,3}\delta V_{PCM,3}\right)c_{p(eff)PCM,3}\frac{\partial T_{PCM,3}}{\partial \tilde{t}}=\begin{bmatrix}U_{PCM,2-PCM,3}\left(T_{PCM,2}-T_{PCM,3}\right)\\-U_{PCM,3-PCM,4}\left(T_{PCM,3}-T_{PCM,4}\right)\end{bmatrix}\delta z\delta x \tag{2.7}$$

$$\left(\rho_{(eff)PCM,4}\delta V_{PCM,4}\right)c_{p(eff)PCM,4}\frac{\partial T_{PCM,4}}{\partial \tilde{t}}=\begin{bmatrix}U_{PCM,3-PCM,4}\left(T_{PCM,3}-T_{PCM,4}\right)\\-U_{PCM,4-PCM,5}\left(T_{PCM,4}-T_{PCM,5}\right)\end{bmatrix}\delta z\delta x \tag{2.8}$$

$$\left(\rho_{(eff)PCM,5}\delta V_{PCM,5}\right)c_{p(eff)PCM,5}\frac{\partial T_{PCM,5}}{\partial \tilde{t}}=\begin{bmatrix}U_{PCM,4-PCM,5}\left(T_{PCM,4}-T_{PCM,5}\right)\\-U_{PCM,5-air}\left(T_{PCM,5}-T_{air}\right)\end{bmatrix}\delta z\delta x \tag{2.9}$$

It can be considered that the specific heat at the inlet and the outlet of the air channel remain the same because of the low range temperature operating condition. The energy balance on the air channel is given as:

$$\begin{aligned}\left(\rho_{air}c_{p,air}\right)\frac{\partial T_{air}}{\partial \tilde{t}}\delta z\delta x\delta y=&\left[U_{PCM,5-air}\left(T_{PCM,5}-T_{air}\right)-U_{air-ins}\left(T_{air}-T_{ins}\right)\right]\delta z\delta x\\&+m_{air}c_{p,air}T_{air,inlet}-m_{air}c_{p,air}T_{air,outlet}\end{aligned} \tag{2.10}$$

Since the temperature at the outlet of the control volume $T_{air,outlet}$ is not directly known. It can be converted into the nodal temperature and the inlet temperature using the approximation: $T_{air}=0.5[T_{air,inlet}+T_{air,outlet}]$ or $T_{air,outlet}=2T_{air}-T_{air,outlet}$. The convective

heat loss coefficient in the air channel is calculated using $h_{conv,air} = \frac{\kappa_{air} Nu}{D_h / 2}$. The hydraulic diameter is divided by two because $h_{conv,air}$ is referenced from the center of the channel to either side. It is given by: $D_h = 2ab/(a+b)$. The Nusselt number is given for constant heat flux, rectangular channel, and fully developed flow condition i.e. $Nu = 8.235\left[1-1.893(b/a)+3.76(b/a)^2-5.814(b/a)^3+5.316(b/a)^4-2(b/a)^5\right]$ (Iv & Lienhard, 1986; Jesumathy et al., 2012).

Finally, an energy balance on the back insulation can be written as:

$$\left(\rho_{ins}\delta V_{ins}\right)c_{p,ins}\frac{\partial T_{ins}}{\partial \tilde{t}} = \begin{bmatrix} U_{air-ins}\left(T_{air}-T_{ins}\right) \\ -h_{conv,ins-amb}\left(T_{ins}-T_{amb}\right)-h_{rad,ins-sky}\left(T_{ins}-T_{sky}\right)\end{bmatrix}\delta z\delta x \qquad (2.11)$$

The convective heat transfer coefficient from the insulation to the ambient is calculated using: $h_{conv,ins-amb} = 5.8+3.7v_{wind}$ (Jesumathy et al., 2012) and the radiative heat loss coefficient from the insulation to the ambient is calculated using: $h_{rad,ins-sky} = \varepsilon_{ins}\sigma\left[T_{ins}+T_{sky}\right]\left[T_{ins}^2+T_{sky}^2\right]$ (McAdams, 1954).

2.1.1 Numerical setup

The developed mathematical equations are formulated numerically using first-order accurate, explicit, time-marching forward finite difference formulation. The discretized formulation:

$$\frac{\partial T_{PV}}{\partial \tilde{t}} = \frac{T_{PV}^{i\,\boxed{n+1}} - T_{PV}^{i\,\boxed{n}}}{\Delta\tilde{t}};\frac{\partial T_{back\ plane}}{\partial \tilde{t}} = \frac{T_{back\ plane}^{i\,\boxed{n+1}} - T_{back\ plane}^{i\,\boxed{n}}}{\Delta\tilde{t}};\frac{\partial T_{PCM,1}}{\partial \tilde{t}} = \frac{T_{PCM,1}^{i\,\boxed{n+1}} - T_{PCM,1}^{i\,\boxed{n}}}{\Delta\tilde{t}};$$
$$\frac{\partial T_{PCM,2}}{\partial \tilde{t}} = \frac{T_{PCM,2}^{i\,\boxed{n+1}} - T_{PCM,2}^{i\,\boxed{n}}}{\Delta\tilde{t}};\frac{\partial T_{PCM,3}}{\partial \tilde{t}} = \frac{T_{PCM,3}^{i\,\boxed{n+1}} - T_{PCM,3}^{i\,\boxed{n}}}{\Delta\tilde{t}};\frac{\partial T_{PCM,4}}{\partial \tilde{t}} = \frac{T_{PCM,4}^{i\,\boxed{n+1}} - T_{PCM,4}^{i\,\boxed{n}}}{\Delta\tilde{t}}; \qquad (2.12)$$
$$\frac{\partial T_{PCM,5}}{\partial \tilde{t}} = \frac{T_{PCM,5}^{i\,\boxed{n+1}} - T_{PCM,5}^{i\,\boxed{n}}}{\Delta\tilde{t}};\frac{\partial T_{air}}{\partial \tilde{t}} = \frac{T_{air}^{i\,\boxed{n+1}} - T_{air}^{i\,\boxed{n}}}{\Delta\tilde{t}};\frac{\partial T_{ins}}{\partial \tilde{t}} = \frac{T_{ins}^{i\,\boxed{n+1}} - T_{ins}^{i\,\boxed{n}}}{\Delta\tilde{t}}$$

are plugged into the mathematical model. After an extensive mathematical derivation, the following matrix is evolved which can give the temperature plots provided it is converged.

$$\begin{bmatrix} A_1 & A_2 & 0 & 0 & 0 & 0 & 0 & 0 & 0 \\ A_3 & A_4 & A_5 & 0 & 0 & 0 & 0 & 0 & 0 \\ 0 & A_6 & A_7 & A_8 & 0 & 0 & 0 & 0 & 0 \\ 0 & 0 & A_9 & A_{10} & A_{11} & 0 & 0 & 0 & 0 \\ 0 & 0 & 0 & A_{12} & A_{13} & A_{14} & 0 & 0 & 0 \\ 0 & 0 & 0 & 0 & A_{15} & A_{16} & A_{17} & 0 & 0 \\ 0 & 0 & 0 & 0 & 0 & A_{18} & A_{19} & A_{20} & 0 \\ 0 & 0 & 0 & 0 & 0 & 0 & A_{21} & A_{22} & A_{23} \\ 0 & 0 & 0 & 0 & 0 & 0 & 0 & A_{24} & A_{25} \end{bmatrix} \begin{bmatrix} T_{PV}^{\,i\ \boxed{n+1}} \\ T_{back\ plane}^{\,i\ \boxed{n+1}} \\ T_{PCM,1}^{\,i\ \boxed{n+1}} \\ T_{PCM,2}^{\,i\ \boxed{n+1}} \\ T_{PCM,3}^{\,i\ \boxed{n+1}} \\ T_{PCM,4}^{\,i\ \boxed{n+1}} \\ T_{PCM,5}^{\,i\ \boxed{n+1}} \\ T_{air}^{\,i\ \boxed{n+1}} \\ T_{ins}^{\,i\ \boxed{n+1}} \end{bmatrix} = \begin{bmatrix} C_1 \\ C_2 \\ C_3 \\ C_4 \\ C_5 \\ C_6 \\ C_7 \\ C_8 \\ C_9 \end{bmatrix} \tag{2.13}$$

2.1.2 Performance metrics of energy analysis

The net-monthly-electrical-power-production of the PVT-air-PCM is calculated by subtracting the electrical consumption from the blower from the monthly-electrical-power-production. It is given by:

$$NMEPP = \sum_{\text{first day of the month}}^{\text{last day of the month}} \overbrace{\left[A \times EPP_{PV} - CEP_{blower}\right]_{day}}^{\text{net electricity production}} \times 10^{-3} \tag{2.14}$$

The area of a photovoltaic panel A is multiplied with EPP_{PV} to express the units of the term $A \times EPP_{PV}$ in W. The term CEP_{blower} is the electricity consumption by the blower and its calculation procedure is mentioned in the author's previous work (Rasikh Tariq & Sheikh, 2018). The term $\left[A \times EPP_{PV} - CEP_{blower}\right]$ represents the net electricity production by the photovoltaic assembly. Finally, it is multiplied with 10^{-3}; thus, $NMEPP$ is expressed in kW. h (Stropnik & Stritih, 2016).

This performance parameter characterizes the heat gain to the air across the thermal collector (called monthly-thermal heat gain) which can be accumulated over the whole year. It is calculated using:

$$MTHG = \sum_{\text{first day of the month}}^{\text{last day of the month}} m_{air} c_{p,air} \left[T_{air,outlet} - T_{air,inlet} \right]_{day} \times 10^{-3} \tag{2.15}$$

Each of the electrical and the thermal part of the collector is characterized based on its efficiency. The monthly-averaged electrical efficiency is defined as the net electrical energy production per unit of the input heat gain for the whole year. It can be written as:

$$\eta_{energetic,monthly,electrical} = 100 \times \sum_{\text{first day of the month}}^{\text{last day of the month}} \left[\frac{A \times EPP_{PV} - CEP_{blower}}{I_T} \right]_{day} \tag{2.16}$$

The monthly thermal efficiency $\eta_{energetic,monthly,thermal}$ is defined as the total thermal heat gain per unit of the input heat gain from the solar radiation, written as:

$$\eta_{energetic,monthly,thermal} = 100 \times \sum_{\text{first day of the month}}^{\text{last day of the month}} m_{air} c_{p,air} \left[\frac{T_{air,outlet} - T_{air,inlet}}{I_T} \right]_{day} \tag{2.17}$$

2.3 Entropy

The yearly averaged entropy generation rate of the collector can be obtained using:

$$\text{Yearly entropy generation} = \sum_{day=1}^{365} \left[\frac{\dot{E}x_{loss}}{T_{amb}} \right]_{day} \tag{2.18}$$

2.2 Exergy analysis

The exergy viewpoint gives the usefulness of the energy analysis; thus, enhancing its applicability. It can be developed for a PVT-air-PCM collector by utilizing net exergy balance on the overall control volume which can include three different rates of exergy i.e. the rate of exergy at the inlet, the rate of exergy at the outlet, and the rate of exergy

loss. The objective of exergy analysis is to find the exergy losses in the PVT-air-collector. Considering, the inlet exergy of the control volume to be positive and the outlet exergy to be negative, the exergy balance can be written as:

$$\dot{E}x_{loss} = \dot{E}x_{sun} - \dot{E}x_{EPP} - \left(\dot{E}x_{air,out} - \dot{E}x_{air,in} \right) \tag{2.19}$$

The terms appearing in this equation are calculated as follows:

1 The radiation exergy rate which is an input to the collector can be computed by applying the theorem of (Petela, 2003, 2008) as: $\dot{E}x_{sun} = I_T A_{PV} \left[1 - \frac{4}{3}\left(\frac{T_{amb}}{T_{sun}} \right) + \frac{1}{3}\left(\frac{T_{amb}}{T_{sun}} \right)^4 \right]$.

2 The electrical power production from the photovoltaic panel is a pure form of energy and it is a useful rate of work. Therefore, the net electrical power production multiplied by the area of the PV panel is actually $\dot{E}x_{EPP}$. Thus, $\dot{E}x_{EPP} = A_{PV} \times EPP - CEP_{blower}$.

3 The exergy flow $\left(\dot{E}x_{air,out} - \dot{E}x_{air,in} \right)$ is calculated using the enthalpy and entropy at the inlet and outlet state points of the collector using: $\dot{E}x_{air,out} - \dot{E}x_{air,in} = m_{air} c_{p,air} \left[\left(T_{air,out} - T_{air,in} \right) - T_{amb} \ln\left(T_{air,out} / T_{air,in} \right) \right]$

The exergy rate equation can be written in terms of the whole year as follows:

$$\dot{E}x_{loss,yearly} = \sum_{day=1}^{365} \left[\dot{E}x_{sun} - \dot{E}x_{EPP} - \left(\dot{E}x_{air,out} - \dot{E}x_{air,in} \right) \right]_{day} \tag{2.20}$$

The equation is accumulated over time; therefore, the units of $\dot{E}x_{loss,yearly}$ are W. h.

The yearly exergetic efficiency is written as:

$$\eta_{exergetic,yearly} = 100 \times \sum_{day=1}^{365} \left[\frac{\dot{E}x_{EPP} + \left(\dot{E}x_{air,out} - \dot{E}x_{air,in} \right) / \text{correction factor}}{\dot{E}x_{sun}} \right]_{day} \quad (2.21)$$

The flow exergy is divided by the correction factor to bring the equivalence owing to the electrical power production and the thermal heat. It signifies that the correction factor is the heat-to-electricity conversion efficiency which, by average, is 35% among Mexican power plants (*Electricity Sector Outlook 2017-2031, Secretaria de Energia (SNER), Mexico*, 2017).

2.4 Exergetic sustainability index

The efficient use of energy resources for a minimum environmental footprint and maximum social ease can ensure sustainable development. In this regard, exergy analysis serves as a systematic approach to reduce the negative impact of overconsumption of available energy resources. It is defined as follows:

$$\text{Exergetic sustainability index} = \frac{1}{1 - \eta_{exergetic,yearly}} \quad (2.22)$$

It is desired to have a PVT-air-collector having a higher exergetic sustainability index.

2.5 Life Cycle emissions of CO_2

The environmental analysis is accompanied by the life-cycle analysis which yields that the CO_2 emission factor for the solar collector which is 4.35×10^{-2} kg_{CO2}. $kW^{-1}.h^{-1}$ (Milousi et al., 2019). The life-cycle CO_2 emissions of the collector can be calculated using:

$$\text{Life cycle emissions of } CO_2 = \text{Emission factor of } CO_2 \times \sum_{\text{first month}}^{\text{last month}} \left(NMEPP + \frac{MTHG}{\text{correction factor}} \right)_{month} \quad (2.23)$$

2.6 Enviroeconomic factor

CO_2, being an element of having global warming potential, therefore, carbon pricing can be an effective method to cut its emissions. In this regard, enviroeconomic analysis is defined as:

$$\text{Enviroeconomic parameter} = \text{Life cycle emissions of } CO_2 \times \text{Emission price of } CO_2 \tag{2.24}$$

(Caliskan, 2017) reported that the emission price of CO_2 is 0.0145 USD. kg^{-1}_{CO2} ($0.28 MXN. kg^{-1}_{CO2}).

2.7 Exergoenvironmental factor

The exergoenvironmental analysis is like the conventional environmental analysis where the energy consumption duration is accounted for. However, the exergoenvironmental considers the exergetic usefulness-based CO_2 value is written as:

$$\text{Exergoenvironmental parameter} = \text{Emission factor of } CO_2 \times \sum_{\text{first month}}^{\text{last month}} \left(\dot{E}x_{EPP} + \frac{\dot{E}x_{air,out} - \dot{E}x_{air,in}}{\text{correction factor}} \right)_{month} \tag{2.25}$$

2.8 Exergoenviroeconomic factor

The exergoenviroeconomic factor is an amalgam of enviroeconomic (cost of carbon pricing) and exergoenvironmental factor. It is a new tool to assess the CO_2 emission considering the exergetic results of the system Therefore, this parameter not only includes the first law of thermodynamics but the second law of thermodynamics, as well. It is given by:

$$\text{Exergoenviroeconomic parameter} = \text{Exergoenvironmental parameter} \times \text{Emission factor of } CO_2 \tag{2.26}$$

It gives the exergetic price of CO_2 emissions.

2.9 Economic analysis

The economic assessment of the PVT-air-PCM collector is carried out based on the life-cycle-cost, Levelized cost of energy, and the payback period for each of the considered locations. It is given by:

1. The life cycle cost of the PVT-air-collector is calculated through a cost balance over the whole life period. It includes a balance of the initial cost, operation, and management (O&M) cost, energy cost, and the salvage value. It can be written as (Sohani et al., 2018; Sohani & Sayyaadi, 2020):

$$\text{LCC} = \text{-Initial cost - O\&M cost - Replacement cost + Energy cost + Salvage value} \quad (2.27)$$

2. The Levelized Cost of energy can be calculated using the Present Worth of Capital Cost PWCC which only includes the life-cycle costs, given by: $\text{PWCC} = \text{Initial cost + O\&M cost + Replacement cost - Salvage value}$ (Sohani et al., 2018). The PWCC must be converted into a Total Annual Cost TAC to calculate the Levelized cost of energy. Therefore, the Capital Recovery Factor CRF can be used to project the present worth of the capital cost into a total annual cost i.e. $\text{TAC} = \text{CRF} \times \text{PWCC}$ (Raman & Tiwari, 2008). Finally, the Levelized Cost of energy can be calculated using (Tripathy et al., 2017):

$$\text{LCOE} = \text{TAC} \Big/ \sum_{\text{first month}}^{\text{last month}} \left(NMEPP + \frac{MTHG}{\text{correction factor}} \right)_{month} \quad (2.28)$$

3. The third economic indicator is the payback period which refers to the number of years that takes the cash flow to become equal to the cash flow i.e. the breakeven point is achieved. It considers the sum of annual cash flows and the initial investment (Mohammadi et al., 2018). Therefore, the Net Present Value (NPV) is given by (Herrando et al., 2018, 2019):

$$\text{NPV} = \text{-Initial cost + Life cycle saving} \frac{1}{i_{discount} - i_{\text{inflation}}} \left[1 - \left(\frac{1 + i_{\text{inflation}}}{1 + i_{discount}} \right)^{\text{number of years}} \right] \quad (2.29)$$

Eq. (2.29) gives the payback period when the NPV is zero i.e. approaching the breakeven point (Sohani et al., 2017).

The calculation details of initial, O&M, replacement, and salvage costs are presented. The one-time initial cost consists of the equipment cost, transport cost, and installation cost. It is given by:

$$\text{Initial cost} = \text{Equipment cost} + \text{Transport cost} + \text{Installation cost} \quad (2.30)$$

Equipment cost is the price of the entire PVT-air-PCM assembly involving construction specifications (see Table 2.1) and the initial cost is presented in Table 2.2.

Table 2.1. Equipment cost.

No.	Component	Price [MXN-Mexican Pesos]
1	PV cells	$500.00[1,2]
2	Inverter	$1,271.00[1,2]
3	Absorber plate	$120.00[2]
4	Phase changing material	$1825.24[3]
6	Insulation	$300.00[2]
7	Casing	$800.00[2]
8	Structural frame	$1,200.00[2]
9	Blower	$842.81 (Dincer et al., 2017)
10	Air filter	$150.00 [2]
11	Intake air grill	$70.00 [2]
12	Outlet air grill	$90.00 [2]
13	Cables	$600.00[2]
14	Circuit breakers	$800.00[2]
15	Overhead cost	15%
16	Equipment cost	$11,004.41

[1] The scaled-down unit price of PV cells and inverter (considering an array-to-invertor ratio of 1.20).
[2] Quoted from a local manufacturer for the specification's details mentioned in section 4.
[3] The price of PCM is referenced from (Bland et al., 2017) and approximated for the subject case.

Table 2.2. Initial cost.

No.	Item	Cost
1	Equipment cost	$11,004.41
2	Installation cost[1]	$800.00 (Mexico City) $900.00 (Monterrey) $800.00 (Campeche City)
3	Transport cost[1]	$500.00 (Mexico City) $800.00 (Monterrey) $500.00 (Campeche City)
4	Initial cost	$12,304.41 (Mexico City)

	\$12,704.41 (Monterrey) \$12,304.41 (Campeche City)

[1] Quoted from local manufacturers of each city.
[2] Considers the charges of the freight.

The operation and maintenance cost involves the maintenance of the equipment and property taxes. The salary of the operator is different for each location, the annual maintenance cost is 5% to the first annual cost (Rasikh Tariq, Sheikh, et al., 2018), and the property tax is ignorable considering a smaller area of the occupied land. The details are presented in Table 2.3.

Table 2.3. Operation and Maintenance (O&M) cost.

No.	Item	Cost
3	First Annual cost[1]	\$1,355.55 (Mexico City) \$1,399.62 (Monterrey) \$1,355.55 (Campeche City)
4	Annual maintenance cost[2]	\$67.77 (Mexico City) \$69.98 (Monterrey) \$67.77 (Campeche City)
5	O&M cost[3]	\$615.22 (Mexico City) \$635.22 (Monterrey) \$615.22 (Campeche City)

[1] $i_{\text{interest}} = 0.1; \text{CRF} = \frac{i_{\text{interest}}\left(1+i_{\text{interest}}\right)^{\text{number of years}}}{\left(1+i_{\text{interest}}\right)^{\text{number of years}}-1}; \text{First annual cost} = \text{CRF} \times \text{Initial cost}$ (Maatallah et al., 2019; Raman & Tiwari, 2008)

[2] $\text{Annual maintenance cost} = 0.05 \times \text{First annual cost}$ (Rasikh Tariq, Sheikh, et al., 2018)

[3] $\text{O\&M cost} = \text{Annual maintenance cost}\left[\frac{\left(1+i_{\text{interest}}\right)^{\text{number of years}}-1}{i_{\text{interest}}\left(1+i_{\text{interest}}\right)^{\text{number of years}}}\right]$ (Tripathy et al., 2017)

The replacement cost of the material/equipment is evaluated for the phase changing material and invertor. By an approximation, at least two inverters are needed for a photovoltaic panel during its lifetime which can be replaced at its midlife. Similarly, (Mengjie et al., 2017) suggested that the thermal life cycles of PCMs can be lower than 1500 times; therefore, a PCM can be replaced after 4 years. As a result, the cost of both items is included over the life span as prescribed by (Tripathy et al., 2017). As a general observation, the inflation rate of a city influences the future replacement cost. Therefore, the following equation gives the present value of the replacement cost considering the inflation rate (Sohani et al., 2018):

$$\text{Replacement cost} = \text{Invertor cost}\left[\frac{\left(1+i_{\text{inflation}}\right)^{\text{replacement year-1}}}{\left(1+i_{\text{interest}}\right)^{\text{replacement year}}}\right] + \text{PCM cost}\left[\frac{\left(1+i_{\text{inflation}}\right)^{\text{first replacement year-1}}}{\left(1+i_{\text{interest}}\right)^{\text{first replacement year}}}\right] + \ldots\ldots + \text{PCM cost}\left[\frac{\left(1+i_{\text{inflation}}\right)^{\text{last replacement year-1}}}{\left(1+i_{\text{interest}}\right)^{\text{last replacement year}}}\right] \tag{2.31}$$

The average inflation rate of Mexico City, Monterrey, and Campeche City 5.14, 4.69, and 4.53% (INEGI, 2014). The salvage value is the income generated from the equipment at the end of its useful life. It is equal to the 15% (Sohani et al., 2018) of the initial cost whose present value; written in terms of the interest rate, is as follows:

$$\text{Salvage value} = \frac{0.15\times\text{Initial cost}}{\left(1+i_{\text{interest}}\right)^{\text{number of years}}} \tag{2.32}$$

The energy cost is the income generated for the PVT-air-PCM collector by selling the electricity and the thermal heat. The federal electricity commission (CFE) of Mexico has a different type of domestic electricity tariffs c_{el} depending upon the locality and is also variable depending upon the month of the year. Therefore, the averaged tariffs are 0.771 MXN/(kW. h) for Mexico City (plan: 1, limit: basic consumption), 0.794 MXN/(kW. h) for Monterrey and Campeche City (plan: 1C, limit: basic consumption) (CFE (Comision Federal de Electricidad), 2018). The energy generated by the collector is considered equivalent to the amount of heat that can be generated from the combustion of natural gas, merely for the calculation procedures. It c_{ng} is 0.38 MXN/(kW. h) (CRE, n.d.). Naturally, photovoltaic panels degrade over their lifetime; therefore, a degradation rate of 10%, 20%, and 30% is considered in the 0-10, 11-20, and 21-25 years, respectively. Thus, the energy cost can be written as (Kalogirou, 2009):

$$\text{Energy cost} = \frac{\left(1+i_{\text{interest}}\right)^{\text{number of years-1}}}{\left(1+i_{\text{discount}}\right)^{\text{number of years}}}\left[c_{el}\sum_{\text{first month}}^{\text{last month}}\left(NMEPP\right)_{month} + c_{ng}\sum_{\text{first month}}^{\text{last month}}\left(MTHG\right)_{month}\right] \tag{2.33}$$

CHAPTER 3. VALIDATION OF RESULTS

(Su, Jia, Alva, et al., 2017) presented a performance analysis of three different configurations of photovoltaic air collectors. Two of the configurations are equipped with phase changing material and the last configuration is a conventional PVT air collector. The design parameters are presented in Table 3.1 and Table 3.2. The authors carried out the analysis for a typical summer day of Nanjing, China from the duration of 07:00 to 18:00 hours which is presented in Fig. 3.1.

The results of the analysis; given the solar data and the design parameters, are presented in Fig. 3.2. It is reported that our results have high conformity with the results of (Su, Jia, Alva, et al., 2017) for the configuration having upper PCM; since both of them are simulation works. With this confidence, the authors can conclude that the developed model can correctly predict the performance of a PVT-air-PCM collector for further deductions.

Table 3.1. Characteristics of the PVT collectors analyzed by (Su, Jia, Alva, et al., 2017).

Parameter	Value
Length of PV module, m	1.5
Width of the PV module, m	1
Height of pipe, m	0.05
Wind velocity, m. s^{-1}	2
Specific heat capacity of air, kJ. kg^{-1}. K^{-1}	1.005
Mass flow rate of air, kg. s^{-1}	0.05
Thickness of PCM	0.05
$\eta_{PV,ref}$ [-]	0.12
Br [$^oK^{-1}$]	0.0045

Table 3.2. PCM material considered by (Su, Jia, Alva, et al., 2017).

Parameter	Symbol	Value
Temperature of fusion [^oC]	ΔT_{PCM}	28
Latent heat capacity [J. kg^{-1}]	H_{latent}	210000
Specific heat capacity [J. kg^{-1}. K^{-1}]	$c_{p(s)}$ $c_{p(l)}$	2900 2100
Thermal conductivity [W. m^{-1}. K^{-1}]	$k_{p(s)}$ $k_{p(l)}$	0.24 0.15
Density [kg. m^{-3}]	$\rho_{p(s)}$ $\rho_{p(l)}$	860 780

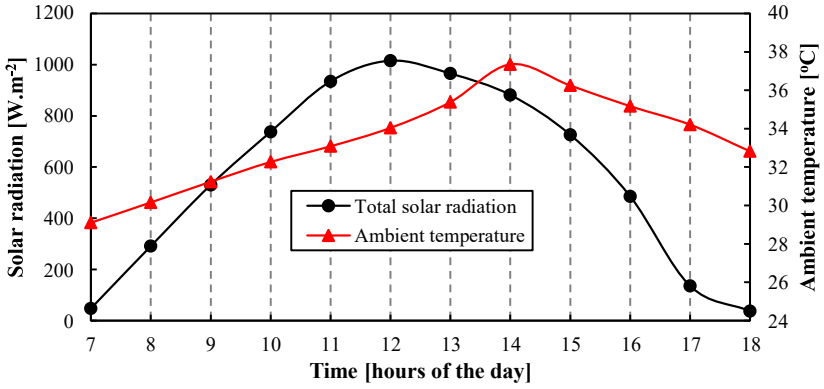

Fig. 3.1. Solar data of Nanjing, China is taken as an input for the analysis of (Su, Jia, Alva, et al., 2017).

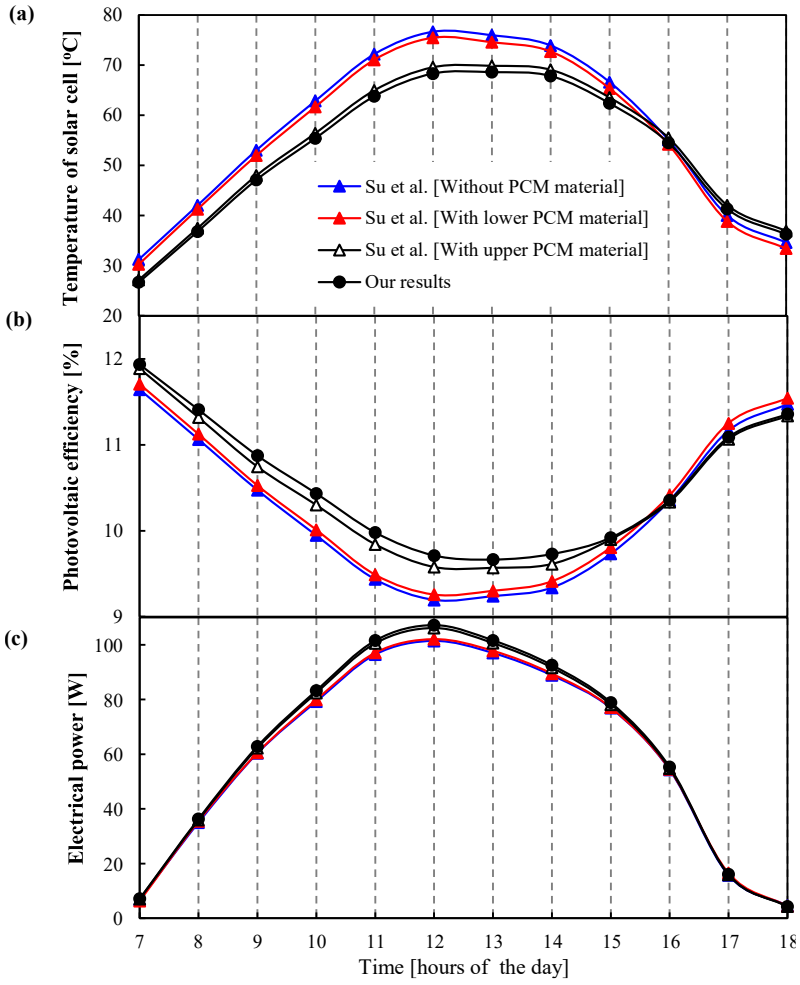

Fig. 3.2. Validation of the current study by comparison with the results of (Su, Jia, Alva, et al., 2017) considering (a) temperature of the solar cell, (b) photovoltaic efficiency, and (c) electrical power.

CHAPTER 4. SIMULATION DETAILS

The prime focus of this work is to analyze the PVT-air-PCM collector for the Mexican climatic conditions. As per Köppen's climate classification (Kottek et al., 2006), Mexico has 15 climatic zones and the dominant are Aw, BWk, BWh, BSh, Cwb, and BSk. However, the population is unevenly distributed in the country where the climatic zones BWk, BSk, and BWh are underpopulated and climatic zone: Cwb; Mexico City, is densely populated. Therefore, the work considers three climatic zones (Aw, BSh, and Cwb) to cover the maximum Mexican territory along with the population-dense regions. The selected cities are Mexico City (19.4326° N, 99.1332° W), Monterrey (25.6866° N, 100.3161° W) and Campeche City (19.8301° N, 90.5349° W) which are in climatic zones Cwb (highland), BSh (semi-arid), and Aw (Savana) respectively. The collector is assumed to be south-facing and is placed at an optimal tilt angle i.e. Mexico City: 17^{o} (Jacobson & Jadhav, 2018), Monterrey: 22.6^{o} (Charles R., 2017a), Campeche: 17.2^{o} (Charles R., 2017b).

Representative weather data of each month (Duffie & Beckman, 2013) of the whole year for each location is extracted from TRNSYS (Klein, 2010) and it is presented in Fig. 4.1. From observation, it is reported that Campeche City has the highest ambient temperature and solar radiation, followed by Monterrey and Mexico City.

The analysis considers a selection procedure of different phase-changing materials and their thermophysical parameters are presented in Table 4.1. Similarly, the thermophysical parameters of the photovoltaic panel, backplane, air channel, and the insulation are presented in Table 4.2.

Table 4.1. Thermophysical properties of phase-changing materials.

Parameter	Symbol		RT35HC [2]		RT28HC[3]		RT25HC[4]	
Temperature of fusion [^{o}C]	ΔT_{PCM}		34-36		27-29		22-26	
Latent heat capacity [J. kg^{-1}]	H_{latent}		240000		250000		210000	
Specific heat capacity [J. kg^{-1}. K^{-1}]	$c_{p(s)}$	$c_{p(l)}$	2000	2000	2000	2000	2000	2000
Thermal conductivity [W. m^{-1}. K^{-1}]	$k_{p(s)}$	$k_{p(l)}$	0.2	0.2	0.2	0.2	0.2	0.2
Density [kg. m^{-3}]	$\rho_{p(s)}$	$\rho_{p(l)}$	880[2]	770[2]	880	770	880	770
Thickness [m]	t_{PCM}		0.03[1]					

[1] Optimal thickness as reported by (Su, Jia, Alva, et al., 2017).
[2] (Abdelrahman et al., 2019; Kant et al., 2016)
[3] (*Data Sheet RT28HC Rubitherm Technologies GmbH Imhoffweg 6 D-12307 Berlin E-Mail: Info@rubitherm.Com Internet: Www.Rubitherm.Com.*, 2020)
[4] (*Data Sheet RT25HC Rubitherm Technologies GmbH Imhoffweg 6 D-12307 Berlin E-Mail: Info@rubitherm.Com Internet: Www.Rubitherm.Com.*, 2020)

Table 4.2. Thermophysical properties of a photovoltaic panel, backplane, air channel, and insulation.

Parameter	Value	Reference
Photovoltaic panel[1]		
Length [m]	1.96	(*PerfectHome Solar Panels*, 2020)
Width [m]	0.99	(*PerfectHome Solar Panels*, 2020)
Thickness [m]	0.035	(*PerfectHome Solar Panels*, 2020)
Density [kg.m^{-3}]	2330	(Jones & Underwood, 2001)
Thermal conductivity [W.m^{-1}. K^{-1}]	148	(Lu & Yao, 2007)
Emissivity [-]	0.91	(Hammami et al., 2017)
Specific heat [J. kg^{-1}. K^{-1}]	677	(Jones & Underwood, 2001)
Absorptivity [-]	0.8	(Shan et al., 2014)
$\eta_{PV,ref}$ [-]	0.1726	(*PerfectHome Solar Panels*, 2020)
Br [^{o}K^{-1}]	0.004	(*PerfectHome Solar Panels*, 2020)
Back plane[2]		
Thickness [m]	0.0005	(Shan et al., 2013)
Density [kg.m^{-3}]	2698	[4]
Thermal conductivity [W.m^{-1}. K^{-1}]	225.94	[5]
Specific heat [J. kg^{-1}. K^{-1}]	921	[6]
Air channel		
Mass flow rate [kg. s^{-1}]	0.05	(Su, Jia, Alva, et al., 2017)
Height of the channel [m]	0.05	(Su, Jia, Alva, et al., 2017)
Density [kg.m^{-3}]	1.29	[7]
Thermal conductivity [W.m^{-1}. K^{-1}]	0.025	[8]
Specific heat [J. kg^{-1}. K^{-1}]	1004	[9]
Insulation[3]		
Thickness [m]	0.05	(A. Tiwari & Sodha, 2006)
Density [kg.m^{-3}]	120	(Bai & Bai, 2014)
Thermal conductivity [W.m^{-1}. K^{-1}]	0.035	(Greenspec, 2020)
Specific heat [J.kg^{-1}. K^{-1}]	1030	(Greenspec, 2020)

[1] The polycrystalline cells based module (code: PC335-72P) is manufactured by Perfecthome solar panels (*PerfectHome Solar Panels*, 2020).
[2] Material: Aluminum.
[3] Material: Glass mineral wool.
[4] (*Thermtest Instruments, MATERIALS THERMAL PROPERTIES DATABASE*, 2020a)
[5] (*Thermtest Instruments, MATERIALS THERMAL PROPERTIES DATABASE*, 2020b)
[6] (*Thermtest Instruments, MATERIALS THERMAL PROPERTIES DATABASE*, 2020b)
[7] (*Thermtest Instruments, MATERIALS THERMAL PROPERTIES DATABASE*, 2020b)
[8] (*Thermtest Instruments, MATERIALS THERMAL PROPERTIES DATABASE*, 2020b)
[9] (*Thermtest Instruments, MATERIALS THERMAL PROPERTIES DATABASE*, 2020b)

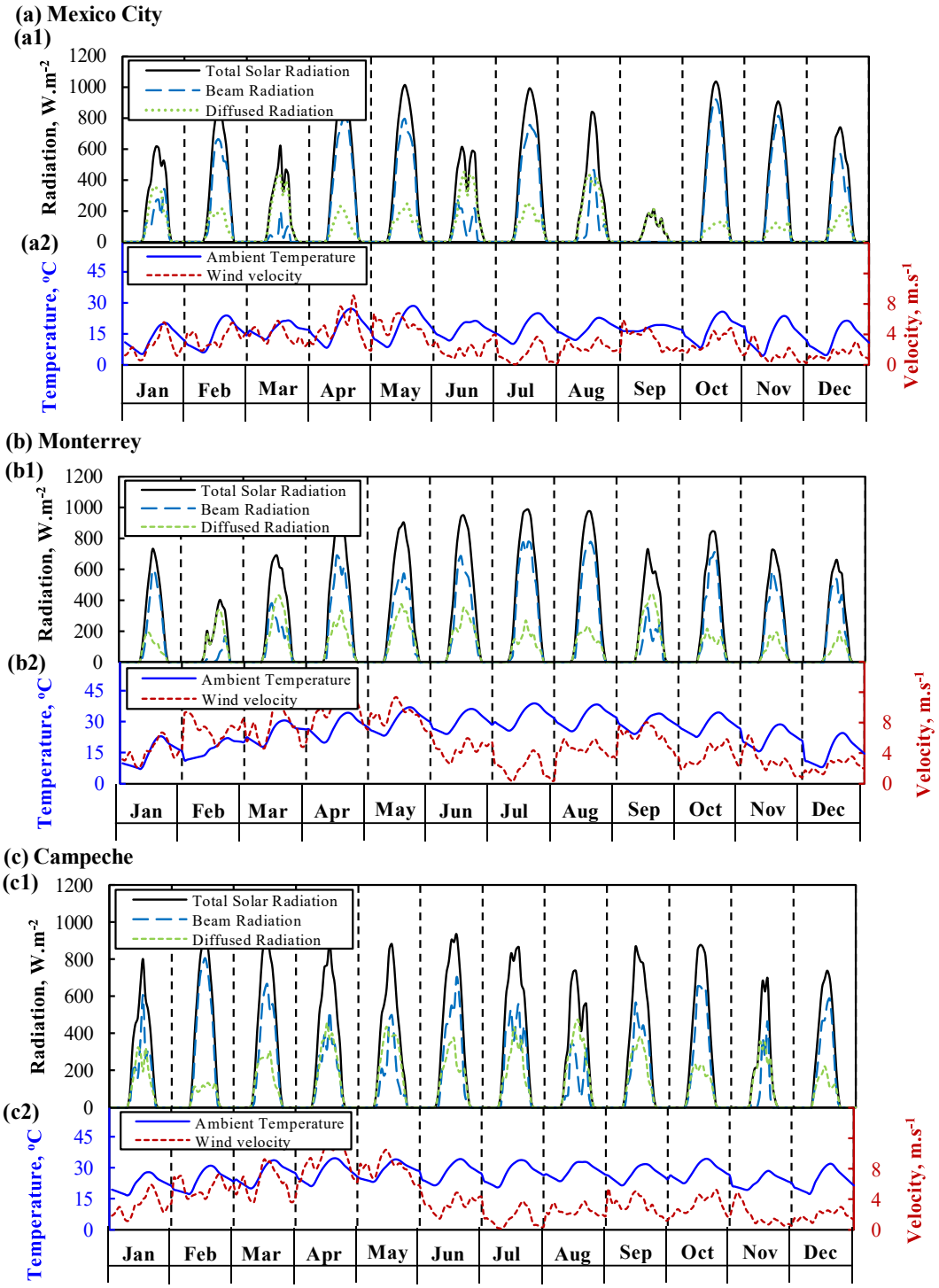

Fig. 4.1 Distribution of (a1) Solar radiation, (a2) ambient temperature and wind velocity, of Mexico City, (b1) solar radiation, (b2) ambient temperature and wind velocity, of Monterrey, (c1) solar radiation, and (c2) ambient temperature and wind velocity of Campeche City.

CHAPTER 5. RESULTS AND DISCUSSION

5.1 Selection of the most suitable phase-changing material

Understandably, each climatic zone has a unique climatic characteristic formed by its elevation, location, ambient temperature, solar radiation, wind velocity, humidity among too many other factors. As a result, a PCM having known thermophysical characteristics (fusion point, specific heat, thermal conductivity, latent heat) can or cannot be suitable to the unique climatic dynamics of a location. Hence, it is quite important to select the right PCM for the right climate. Thus, in this section, a systematic selection procedure of the phase-changing material is presented for each of the city considering its variant climatic behavior. Simulations are carried out on three different PCMs (RT35HC, RT28HC, and RT25HC) for each of the city (Mexico City, Monterrey, and Campeche) and the results are presented in Fig. 5.1. The analysis is supported by the melting percentage of each PCM to justify its physics for each climatic dynamic.

Fig. 5.1(a1, b1, and c1) shows the temperature of the photovoltaic panel without PCM along with PCM RT35HC, RT28HC, and RT25HC supported with the ambient temperature and the solar radiation for each month of the whole year. It is reported that for each day the photovoltaic temperature with and without PCM is increasing with the increase in solar radiation, and similarly, decreasing with the decrease in solar radiation because the solar radiation is a source of thermal energy to the photovoltaic panel. Particularly, for the case of PV without PCM, before the sunshine hours, the PV temperature is equal to the ambient temperature due to the solution of energy balance equations. It remains the same until the solar radiation is absorbed by it, reaching a maximum at the peak of ambient temperature, and dropping back to the ambient temperature in the absence of solar radiation. Thus, the peaks of photovoltaic temperature; regardless of the existence of PCM, coincides with the peaks of ambient temperature. This makes quite a sense because the thermal potential is minimum during the peak ambient temperature; thus, an expected elevated PV temperature is observed. The pattern is followed throughout the whole year which can also be affected by wind velocity. For example: in the case of Mexico City, the high wind velocity and

low solar radiation during September decreases the PV temperature owing to a dominant wind-induced cooling.

Fig. 5.1(a1) presents the PV temperature with different phase changing materials for Mexico City. Surprisingly, the PV temperature by using PCM RT35HC in Mexico City gives a higher photovoltaic temperature; ~8% more as compared to the photovoltaic temperature without the use of any PCM. The results are quite contradictory because it is reported from the literature that PCM should contribute to the thermal management of the PV panel. However, the authors emphasize that the thermal management of PV panels using PCM is only possible through a suitable PCM selection. This process is explained by the fact as presented in Fig. 5.1(a2) that the melting percentages of PCM RT35HC are quite less averaging to only ~2.5% for the whole year corresponding to the fact that the PCM mostly remained in its solid-state and has an inherited lower thermal conductivity, and thus, acting as an insulation to the PV temperature leading to a higher PV temperature as compared to the case of without PCM. The PCM remained in its solid-state because it has a higher fusion range Thus, in other words, the local climatic dynamics could not generate enough heating to the PV panel to exploit the latent heat energy of PCM RT35HC.

Fig. 5.1(a1) also illustrates the PV temperature for the case of a collector using PCM RT28HC and PCM RT25HC. The lowest PV temperature is observed for the case of PCM RT25HC, followed by PCM RT28HC corresponding to ~17.2% and ~11% yearly averaged temperature decrement, respectively. It is explained through the melting percentages of each PCM which is the highest for RT25HC at a yearly averaged value of ~26%. It signifies that the phase change/latent heat energy of RT25HC is captured more than other PCMs. In summary, the climatic dynamics of Mexico City are only suitable to exploit the phase change energy of a PCM having a lower fusion range like 22-26^{o}C. Thus, PCM RT25HC is recommended for Mexico City.

Several other observations are also made from Fig. 5.1(a1). The solar radiation is the lowest for September. Therefore, the hourly weather dynamics are not enough even to utilize the latent heat of PCM RT25HC. It concludes that the thermal management of PV with PCM is not effective for a duration of lower solar radiation. Similarly, the month

of March exhibits lower ambient temperature resulting in a higher thermal potential from the PV panel to the local environment as compared to the PCM side. Therefore, the melting percentages are also lower for this month. It signifies that the use of PCM for the thermal management of PV is not recommended for climatic zones having a lower ambient temperature. Similarly, the PV thermal management using PCM for a climatic zone having higher wind velocity is not recommended. Additionally, the PCM cannot be suitable for a climatic zone which has very high climatic fluctuations because, in this way, one PCM cannot fully exploit the yearly climatic dynamics. In other words, a PCM can be suitable for the crust of a weather fluctuation and might not melt for the trough of the same weather fluctuation. All of these corresponds to the technical limitations of the PV-PCM combination.

A similar discussion can be deduced from Fig. 5.1(b) in which the most suitable PCM is RT28HC because Monterrey has relatively more solar radiation and ambient temperature from Mexico City. Thus, a PCM having a relatively higher fusion range (27-29^{o}C) utilizes the maximum phase change energy. Wind-induced cooling is more dominant in the case of Monterrey. The first five months from January to May has higher wind velocities as compared to the rest of the year. Thereby, the PV temperatures are relatively lower for the first five months. From the perspective of available solar radiation, the PCM is not effective for the thermal management of PV for Monterrey for February owing to its lower solar radiation. Overall, for Monterrey, the temperature decrement of the PV panel using PCM RT28HC is ~18% as compared to the case of not using a PCM.

Likewise, from Fig. 5.1(c), the most suitable PCM for Campeche City is RT35HC which is a tropical savanna climatic zone, experiences the maximum solar radiation and ambient temperature and remains nearly consistent throughout the year. The month of April and May experiences the maximum wind-induced cooling on the PV surface, and the month of November experiences the minimum solar radiation; therefore, the PV temperatures are lower for these months. Overall, Campeche has the maximum solar radiation and ambient temperature; thus, making it suitable for a PCM of high fusion range to be fully effective. Hence, the averaged melting ratio of RT35HC is 31%, and

the temperature decrement is around ~20% as compared to the case of not using a PCM.

It is noted that for Monterrey the melting percentage of RT25HC is highest, yet, the lowest PV temperature is observed for RT28HC. Similarly, for Campeche City, the highest melting percentage is of RT25HC, followed by RT28HC, yet, the lowest PV temperature is reported for RT35HC. It is explained by the thermophysical characteristics of each PCM and its association with the region climatic dynamics. First, RT25HC has the lowest specific heat, by this means, limiting its energy storage capacity knowing that Monterrey and Campeche City have the highest incoming heat in terms of solar radiation. Additionally, the lower fusion range of RT25HC readily presents the PCM to allow an easy phase change process even before the peak ambient temperature when the thermal management is needed the most. Therefore, a higher melting percentage (>70%) can also constraint the thermal management because, in this way, a lower quantity of the material is left for energy storage. In conclusion, lower melting percentages of PCM cannot fully avail the latent heat, and higher melting percentages leave a lower thermal mass for energy storage. As a result, RT28HC and RT35HC are recommended for Monterrey and Campeche City.

Some other general observations are made from Fig. 5.1. In a comparison of all three locations, Campeche City has shown the highest PV temperature, followed by Monterrey and Mexico City. However, Campeche City has shown the maximum decrement in the PV temperature owing to its consistency in the climatic pattern. Some other observations are that for the case of using a PCM, regardless of the location, the PV temperature takes a suitable time to return the ambient temperature. However, the PV without PCM reaches the ambient temperature more quickly than the PV with PCM. It makes sense because the solidification process of the PCM emits heat. Additionally, Campeche City needs the maximum time for the PCM to reach the solidification, followed by Monterrey and Mexico City.

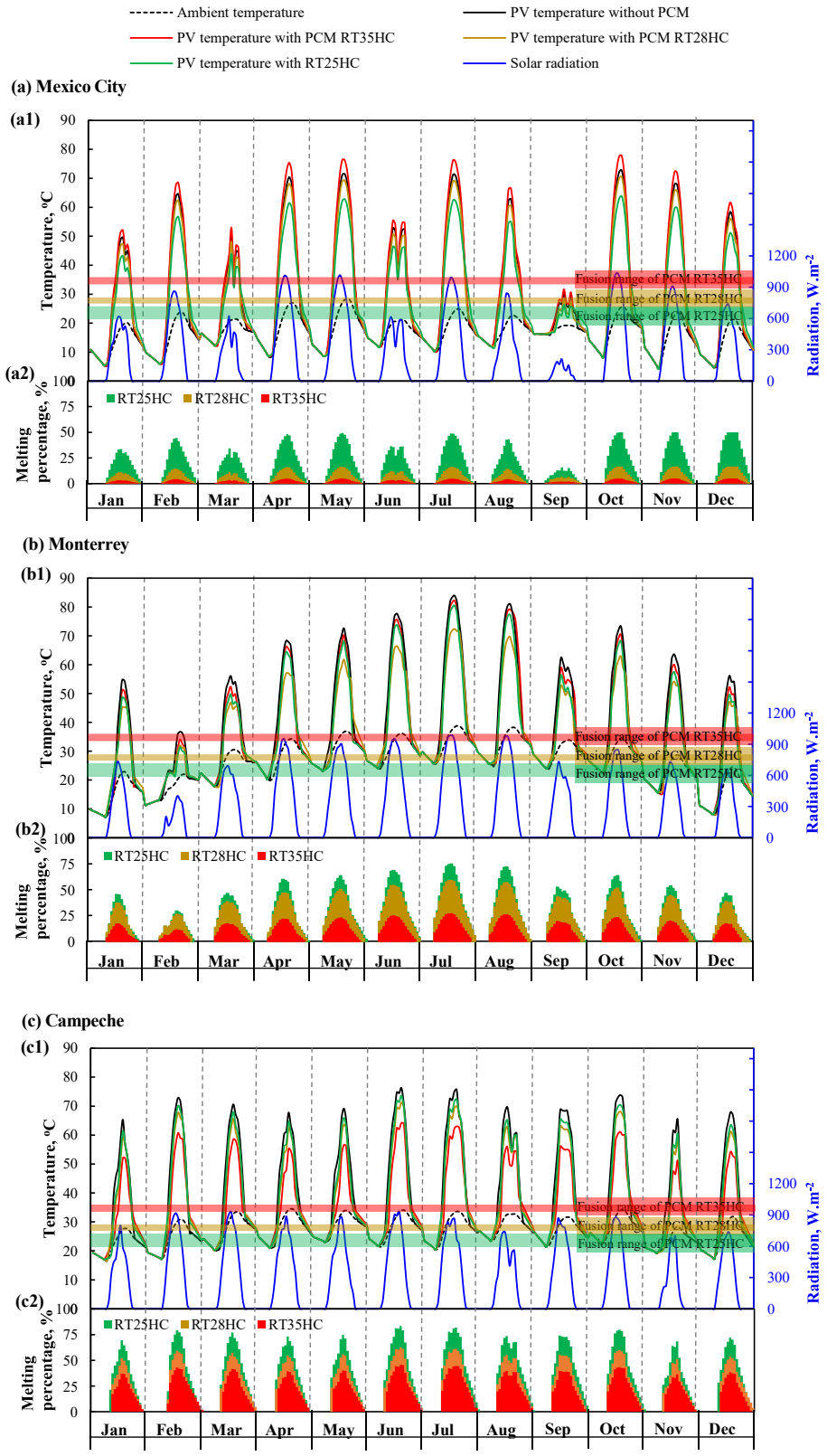

Fig. 5.1. Characteristics of PVT-PCM collector for (a) Mexico City, (b) Monterrey, and (c) Campeche City.

Finally, this analysis can allow us to make a recommendation on the selection of PCM for different climatic zones of Mexico. Fig. 5.2(a) presents the climate classification graph of Mexico adapted from Köppen (Kottek et al., 2006), and Fig. 5.2(b) presents the general recommendation on the selection of PCM for the thermal management of PV panels for the three climatic zones of Mexico.

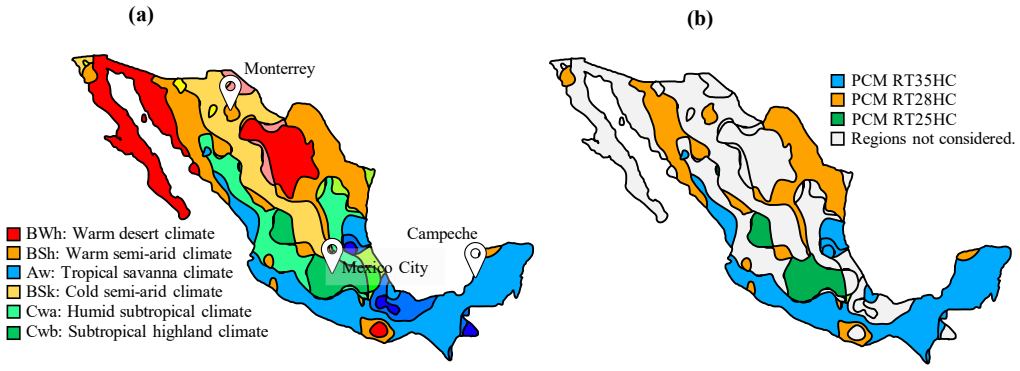

Fig. 5.2. (a) Mexican climatic map adapted from Köppen climate classification (Kottek et al., 2006), and (b) recommendation on the selection of CM subjected to the Mexican climate.

5.2 Yearly simulation results

Fig. 5.3 presents the first-law performance indicators of PVT air collectors (with and without PCM) for each subject location. It presents the net-monthly-electrical-power production, first-law energetic efficiency from PV perspective, monthly-thermal heat gain, and first law energetic efficiency from thermal heat gain perspective.

For Mexico City, Fig. 5.3 (a) and (c) indicate the accumulative net-monthly-electrical production and accumulative monthly thermal heat gain are lowest for January, March, June, and September and highest for April, May, July, and October which perfectly reflects the patterns of the solar radiation presented in Fig. 4.1. Likewise, for Monterrey, the net-monthly-electrical power production and monthly thermal heat gain are lowest for February, November, and December and highest for April, May, June, July, and August as per its weather pattern. For Campeche, apart from January, August, November, and December, the performance indicators are nearly consistent owing to its special climatic pattern.

Fig. 5.3 (b) and (d) presents the first-law definitions of electrical and thermal efficiencies. It is observed that, regardless of the climatic zone, the first-law efficiencies

are maximum for months experiencing lower solar radiation and a minimum for months experiencing higher solar radiation. It makes sense because, for the case of electrical efficiency, the PV heat-to-electricity conversion capacity can be better for lower solar radiation owing to a lower PV operating temperature. However, for the case of thermal efficiency, higher solar radiation is correlated with a higher ambient temperature which decreases the potential of flow heat per unit input solar radiation. For example: For Campeche City, the electrical and thermal efficiency is lowest for June which has the highest solar radiation, and highest for January which has the lowest solar radiation.

Another perspective from Fig. 5.3 is related to the pattern of percentage enhancement of PVT collectors by the usage of PCM. It is realized that the percentage enhancement in the first-law performance indicators is highest for the month of highest solar radiation (for example March to July in Campeche City) because it aids the PCM to function properly in terms of its melting percentage.

Table 5.1 presents the summary of this section in which the yearly accumulated thermal and electrical power, and averaged thermal and electrical efficiencies are presented. The highest first law energy indicators are reported for Mexico City, followed by Monterrey and Campeche which also coincides with the findings of section 5.1.1. The enhancement in the electrical power is 22% for Mexico City (same as Monterrey), followed by Campeche City. Since Monterrey has overall high fluctuation in weather parameters; therefore, it directly reflects in the yearly first-law indicators.

Table 5.1. Summary of the energetic performance indicators for each city with and without the consideration of PCM.

		Mexico City	Monterrey	Campeche
With PCM	Yearly accumulated NMEEP [kW. h]	377.6	446.3	516.1
	Yearly averaged electrical efficiency [%]	8.0	9.1	10.6
	Yearly accumulated MTHG [kW. h]	486.5	575.0	664.9
	Yearly averaged thermal efficiency [%]	25.1	28.7	33.2
Without PCM	Yearly accumulated NMEEP [kW. h]	308.0	364.1	416.0
	Yearly averaged electrical efficiency [%]	6.5	7.5	8.7
	Yearly accumulated MTHG [kW. h]	396.8	469.1	535.9
	Yearly averaged thermal efficiency [%]	20.4	23.5	26.7

Percentage	In yearly accumulated NMEEP [kW. h]	22.6	22.6	24.1
difference	In yearly averaged electrical efficiency [%]	22.9	20.8	22.2
	In yearly accumulated MTHG [kW. h]	22.6	22.6	24.1
	In yearly averaged thermal efficiency [%]	22.9	21.7	24.1

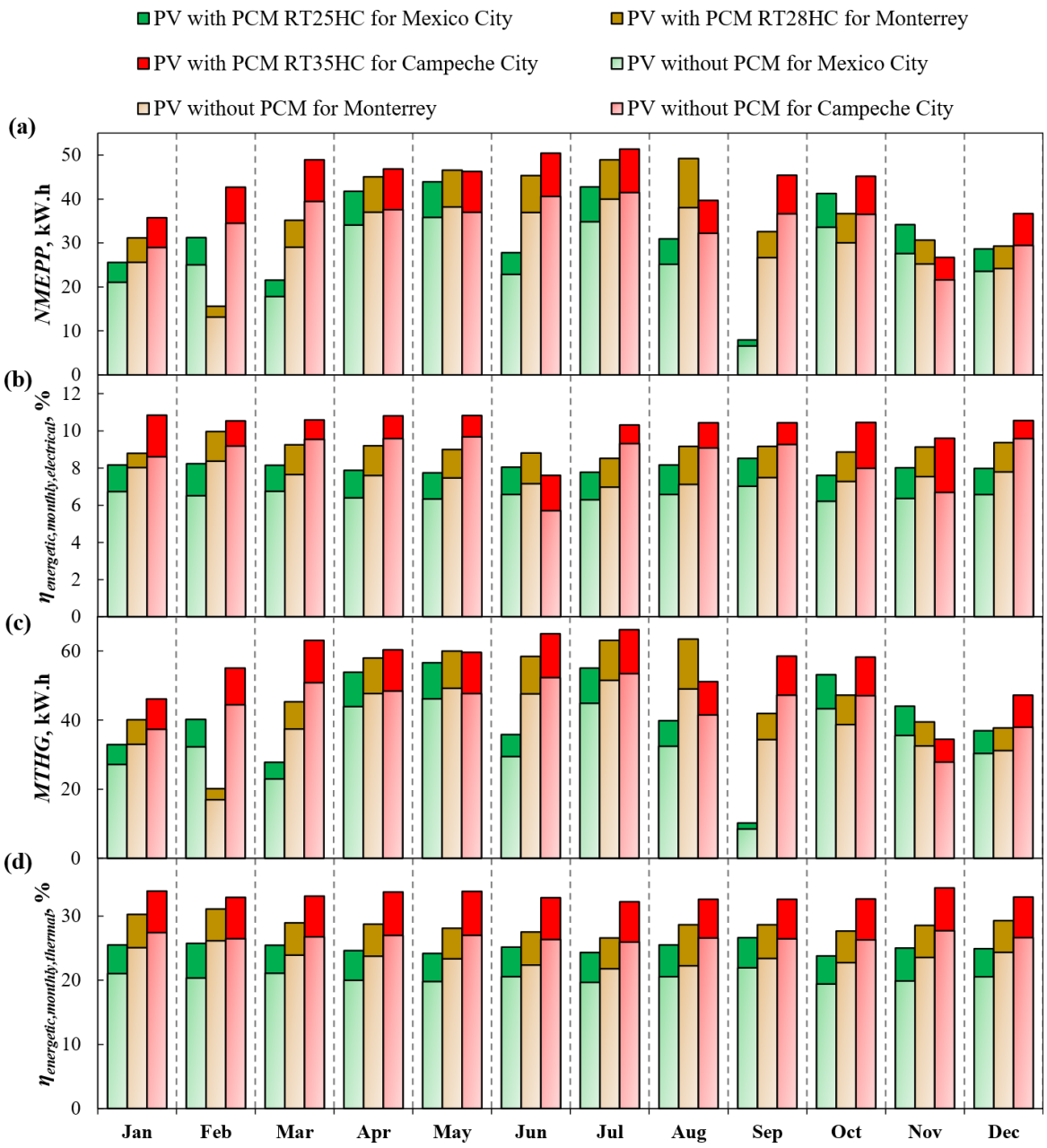

Fig. 5.3. Yearly simulation results of parameters: (a) net-monthly-electrical-power-production, (b) first law electrical efficiency, (c) monthly-thermal heat gain, and (d) first law thermal efficiency, considering the most suitable PCM for Mexico City, Monterrey, and Campeche City.

5.3 Viewpoints from other multi-disciplinary parameters

The results of the yearly accumulated exergy distribution are presented in a Sankey diagram (refer to Fig. 5.4) for each city for the case of PVT-air-PCM. The percentage of total input exergy utilized for PV generation is 9.5, 10.9, and 12.5, flow exergy is 11.7, 13.6, and 15.6, and the energy losses are 78.7, 75.4, and 71.8 for Mexico City, Monterrey, and Campeche City respectively. The highest exergy utilization: in other words, exergetic efficiency (see Fig. 5.4(a)) and yearly entropy generation rate (see Fig. 5.5(a)) is reported for Campeche City, followed by Monterrey and Mexico City.

The exergetic analysis directly reflects the sustainability index (see Fig. 5.5(b)) which is highest for Campeche City (~1.4) considering its lowest entropy generation rate. Additionally, Campeche has the highest energetic (see Fig. 5.5(c)) and exergetic (enviroeconomic: see Fig. 5.5(e)) life cycle CO_2 emissions contributing to a high energetic carbon pricing (enviroeconomic: see Fig. 5.5(d)), and exergetic carbon pricing (exergoenviroeconomic: see Fig. 5.5 (f)).

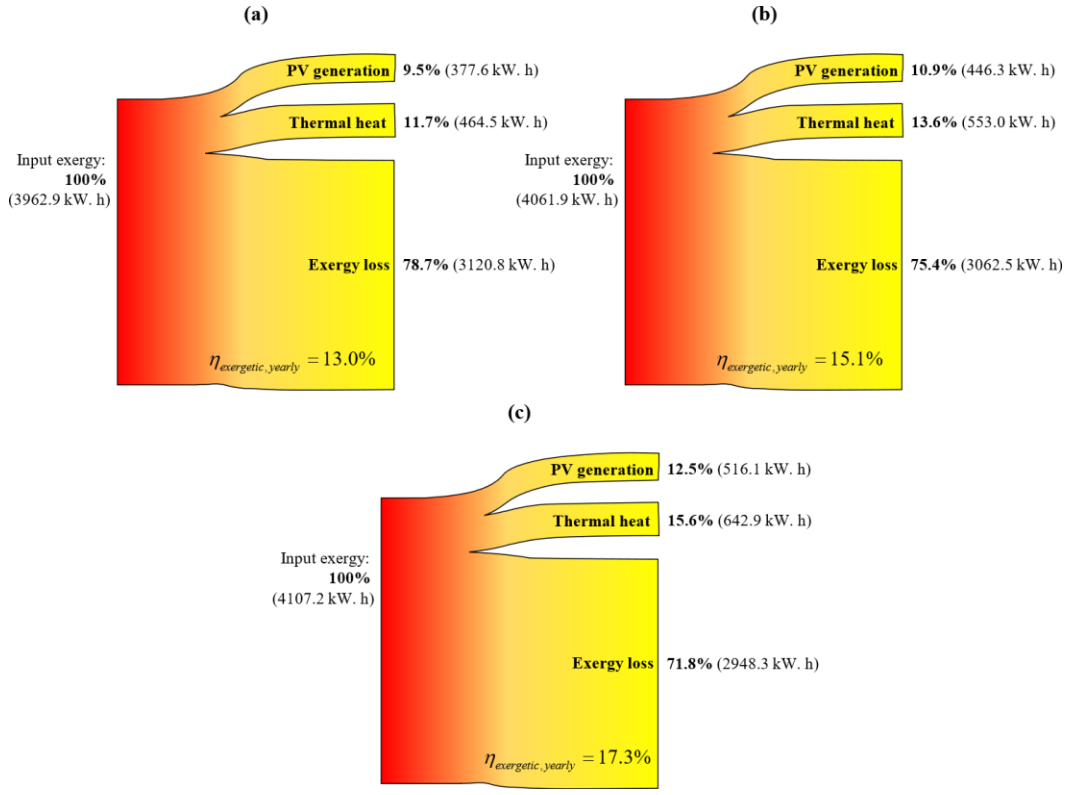

Fig. 5.4. Sankey diagram of exergy distribution for (a) Mexico City, (b) Monterrey, and (c) Campeche City.

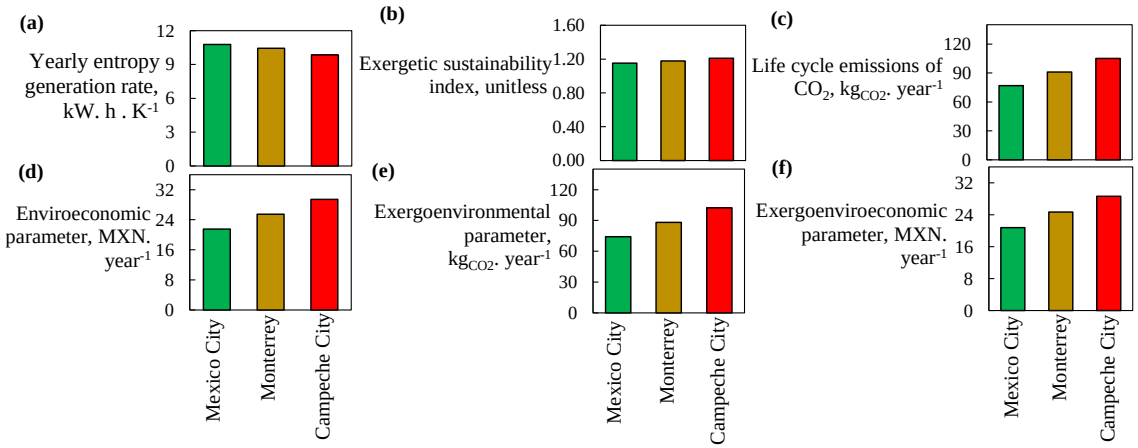

Fig. 5.5. (a) Yearly entropy generation rate, (b) exergetic sustainability index, (c) life cycle emissions of CO_2, (d) enviroeconomic parameter, (e) exergoenvironmental parameter, and (f) exergoenviroeconomic parameter of PVT-air-PCM collector for Mexico City, Monterrey, and Campeche City.

5.4 Economical feasibility

In this section, the results of the economic analysis are presented (see Fig. 5.6). The highest life-cycle-cost is reported for Campeche City, Monterrey, and Mexico City. In other words, the LCC can indicate the profit generated by the collector over its lifetime; therefore, Campeche has significant financial advantages. Mexico City has the highest cost of energy at $4.30 MXN/(kW.h), followed by Monterrey and Campeche City. The payback period of the collector is lowest in Campeche at 10.8 years; although it is a little higher as compared to the one reported in the literature (Al-Waeli et al., 2018). In conclusion from this section, Campeche (climatic zone: Aw) performs the best based economic assessment majorly because of its consistency in climatic behavior.

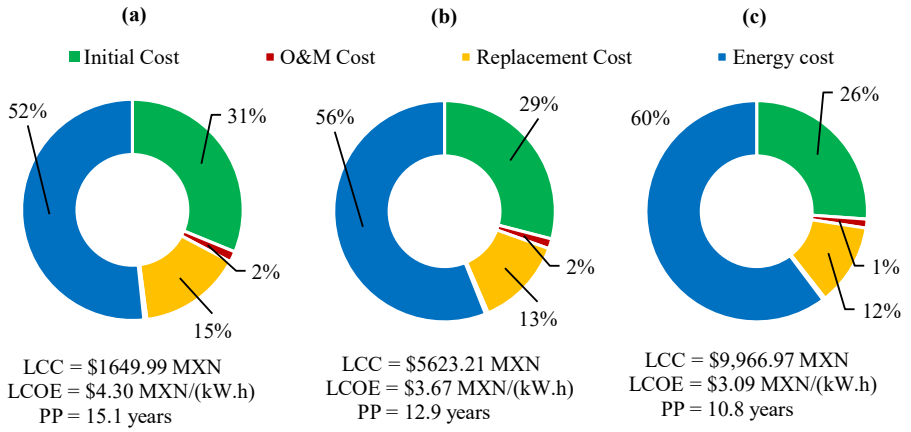

Fig. 5.6. Results of economic analysis for (a) Mexico City, (b) Monterrey, and (c) Campeche City.

5.5 Comparison of results

In this section, the comparison of the result is presented based on the first and second law performance indicators. The prime objective of this section is to review the performance indicators of similar collectors available in the literature and to compare them with our results.

Table 5.2 presents the electrical, thermal and exergetic efficiency of similar collectors which are available in research, and it is deduced that the first and second law efficiencies for Mexico City are lower than the one available in the literature; however, the efficiencies reported for Campeche City are comparable with the other studies.

Table 5.2. Comparison of different collectors based on electrical, thermal, and exergetic efficiency.

Reference	Technology	Electrical efficiency [%]	Thermal efficiency [%]	Exergetic efficiency [%]
(Al-Shamani et al., 2016)	PVT with water[1]	9.142	58.22	-
(Al-Shamani et al., 2016)	PVT with SiO_2 nanofluid[2]	10.09	60.54	-
(Al-Shamani et al., 2016)	PVT with TiO_2 nanofluid[3]	10.58	63.67	-
(Al-Shamani et al., 2016)	PVT with SiC nanofluid[4]	13.07	65.88	-
(Rounis et al., 2016)	Building-integrated PVT[5]	~13.9	~39	-
(G. Li et al., 2015)	PV/T with static miniature solar concentrator[6]	10.1	36.3	
(Sardarabadi et al., 2017)	PV	-	-	10.9
(Sardarabadi et al., 2017)	PVT with deionized water	-	-	12.23
(Sardarabadi et al., 2017)	PVT with ZnO-water nanofluid	-	-	12.29
(Sardarabadi et al., 2017)	PVT-PCM with deionized water	-	-	13.17
(Sardarabadi et al., 2017)	PVT-PCM with ZnO-water nanofluid	-	-	13.42
(Gaur et al., 2017)	PVT with PCM	16.30	~40	-
(Kazemian et al., 2018)	PV	12.91	-	12.27
(Kazemian et al., 2018)	PV with PCM	13.42	-	12.75
(Kazemian et al., 2018)	PVT with PCM	14.03	70.46	14.37
(Hosseinzadeh et al., 2018)	PV	12.56	-	10.73
(Hosseinzadeh et al., 2018)	PVT with nanofluid	13.44	39.86	~12.1
(Hosseinzadeh et al., 2018)	PVT-PCM with nanofluid	14.05	51.66	~13.6
(Fayaz, Rahim, Hasanuzzaman, Nasrin, et al., 2019)	PVT-PCM	12.59	-	-

(Ahn et al., 2015)	PVT collector with heat recovery ventilation	15.0	23	-
(Fayaz et al., 2018)	PVT with MWCNT-nanofluid	12.37	79.1	-
(Fayaz et al., 2018)	PVT with water	12.3	75.24	-
(Jahromi et al., 2015)	PVT	-	52	9.7
(Maatallah et al., 2019)	PVT-PCM	~13.5	~27	-
(Hossain et al., 2018)	PVT-PCM	11.08	87.72	12.19
(Hossain et al., 2018)	PV	9.75		7.01
(J. H. Kim et al., 2014)	PVT air collector	15	22	-
(S. Tiwari et al., 2018)	PVT air collector integrated drying system	11.26	26.68	-
(da Silva & Fernandes, 2010)	PVT	9	15	-
This work	PVT with PCM RT25HC for Mexico City	8.0	25.1	13.0
This work	PVT with PCM RT28HC for Monterrey	9.1	28.7	15.1
This work	PVT with PCM RT35HC for Campeche City	10.6	33.2	17.4

[1] The mass flow rate of the working fluid is 0.068 kg. s^{-1}
[2] The mass flow rate of the working fluid is 0.68 kg. s^{-1}.
[3] The mass flow rate of the working fluid is 0.068 kg. s^{-1}.
[4] The mass flow rate of the working fluid is 0.68 kg. s^{-1}.
[5] Summer, no wind conditions, and a mass flow rate of 400 kg. h^{-1} of the working fluid.
[6] March, 14.

Table 5.3 reports the comparison of the Levelized Cost of the energy of different devices working on a similar principle. The LCOE is higher for the proposed PVT-air-PCM collector owing to its yearly simulation as some of the months can be under-optimized for PCM operation. Anyways, there is a general critic on the economic feasibility of PV-PCM collectors which can be improved provided the PCM and inverter costs can be replaced because they constitute a big portion in life cycle cost analysis (see Fig. 5.6)

Table 5.3. Comparison of different collectors based on the Levelized cost of energy.

Reference	Technology	Location	Cost of energy [USD. kW^{-1}. h^{-1}]
(J. Y. Kim et al., 2009)	PV	Korea	0.531[1]
(Lazard, 2018)	PV	Atlanta	0.412
(J. Y. Kim et al., 2009)	PV	Korea	0.824[2]
(Wang et al., 2019)	PV-ETC	Italy	0.099[3]
(Mondal & Denich, 2010)	PV	Oman	0.327
(Kazem et al., 2017)	PV	Oman	0.2258
(M., 2012)	PV	Oman	0.304

(Celik, 2006)	PV	Turkey	0.440[4]
(Celik, 2006)	PV	Turkey	0.500[5]
(Celik, 2006)	PV	Turkey	0.710[6]
(Celik, 2006)	PV	Turkey	0.950[7]
(Hazi et al., 2014)	PVT	Romania	0.06272[3] for heat 0.0336[3] for electricity
(Tripathy et al., 2017)	Building-integrated PVT	India	1.61-3.61
(Al-Waeli, Kazem, et al., 2019)	PVT with nano-PCM/nanofluid	Malaysia	0.112
(Al-Waeli et al., 2018)	PVT with nanofluid	Malaysia	0.196
(Gu et al., 2018)	PVT concentrator	Sweden	0.14224[3]
(Arıcı et al., 2018)	PV-PCM	Turkey	0.1456[3] to 0.16352[3]
This work	PVT-air-PCM	Mexico	0.1545 to 0.215

[1] With 91% of inverter efficiency.
[2] With 92% of inverter efficiency.
[3] Considering an exchange rate of 1 Euro = 1.12 USD
[4] A PV size of 2 kW, with battery storage and inverter efficiency of 95-98%.
[5] A PV size of 3.034 kW with battery storage.
[6] A PV size of 2 kW without battery storage.
[7] A PV size of 3.034 kW without battery storage.

CONCLUSION

A literature gap is identified that PVT collectors integrated with PCM using air as a working fluid have not gone through extensive research. Additionally, the PV and PCM integration is subject to climatic characteristics; therefore, research is lacking in the proper selection procedure of PCM for the thermal management of PV. And finally, almost no research is available on the entropy, life cycle emissions, enviroeconomic, exergoenvironmental, exergoenviroeconomic, and economic assessment. The work is a unique blend of a classical mathematical model consisting of energy balance, covering the multi-disciplinary thermodynamic indicators, and finalized with an extensive mathematical model. The following are the key findings of this work:

1. PCM selection has the most important role to enhance the thermal performance of PVT devices. This selection procedure is completely dependent on the local climatic dynamics. Improper PCM selection can even rise the PV temperature. Additionally, the PV-PCM combination has a very narrow operating range for its optimality. For example, PCM is not suitable for climatic zones having high-temperature fluctuation, radiation variance, high wind velocity, or cold climates. In conclusion, PCM RT35HC is suitable for tropical Savana climate (Aw), RT28HC for warm semi-arid climate (BSh), and RT25HC for highland (Cwb) climatic zones.
2. For the best-selected PCM, the thermal and electrical efficiencies are 22-33% and 8-10.6%, respectively which are ~20-24% more than the case of not using a PCM. The highest performance enhancement is reported for Savana climatic zone which has a nearly consistent climatic pattern throughout the year.
3. The exergetic losses are very high ranging from 71% to 78% which is caused by the sub-optimal PCM performance for the fluctuation in weather parameters. The exergetic efficiency ranges from ~13 to ~17%. The exergetic sustainability index is around ~1.2.
4. The life cycle CO_2 emissions based on first and second law ranges from 65 to 95 kg per year. CO_2 pricing based on energy and exergy balances ranges from $20.00-$32.00 MXN per year.

5. The Levelized Cost of energy is $4.30 MXN/(kWh), $3.67 MXN/(kWh), and $3.09 MXN/(kWh) for Aw, BSh and Cwb climatic zones. Similarly, the payback period ranges from 10 to 15 years.
6. The capacity factor of the plant for Mexico City, Monterrey, and Campeche City is 0.14, 0.16, 0.19, respectively for the photovoltaic electricity generation.

Although, the theoretical understanding of the photovoltaic thermal collector having air as a working fluid using phase changing material as a heat rejection source is possible; yet, it’s practical realization, especially for a mass industrial scales comes up through a series of problems including the manufacturing complications, installation procedures, operational problems, and the maintenance difficulties. Nevertheless, the system can have successful utilization in building-integrated systems for a case when the secondary use of the system is also important as the need for air heating.

REFERENCES

Abdelrahman, H. E., Wahba, M. H., Refaey, H. A., Moawad, M., & Berbish, N. S. (2019). Performance enhancement of photovoltaic cells by changing configuration and using PCM (RT35HC) with nanoparticles Al2O3. *Solar Energy*. https://doi.org/10.1016/j.solener.2018.11.022

Ahn, J. G., Kim, J. H., & Kim, J. T. (2015). A study on experimental performance of air-type PV/T collector with HRV. *Energy Procedia*, *78*, 3007–3012. https://doi.org/10.1016/j.egypro.2015.11.705

Al-Shamani, A. N., Sopian, K., Mat, S., Hasan, H. A., Abed, A. M., & Ruslan, M. H. (2016). Experimental studies of rectangular tube absorber photovoltaic thermal collector with various types of nanofluids under the tropical climate conditions. *Energy Conversion and Management*. https://doi.org/10.1016/j.enconman.2016.07.052

Al-Waeli, A. H. A., Chaichan, M. T., Sopian, K., Kazem, H. A., Mahood, H. B., & Khadom, A. A. (2019). Modeling and experimental validation of a PVT system using nanofluid coolant and nano-PCM. *Solar Energy*, *177*(October 2018), 178–191. https://doi.org/10.1016/j.solener.2018.11.016

Al-Waeli, A. H. A., Kazem, H. A., Chaichan, M. T., & Sopian, K. (2019). Experimental investigation of using nano-PCM/nanofluid on a photovoltaic thermal system (PVT): Technical and economic study. *Thermal Science and Engineering Progress*, *11*(November 2018), 213–230. https://doi.org/10.1016/j.tsep.2019.04.002

Al-Waeli, A. H. A., Kazem, H. A., Sopian, K., & Chaichan, M. T. (2018). Techno-economical assessment of grid connected PV/T using nanoparticles and water as base-fluid systems in Malaysia. *International Journal of Sustainable Energy*, *37*(6), 558–575. https://doi.org/10.1080/14786451.2017.1323900

Arıcı, M., Bilgin, F., Nižetić, S., & Papadopoulos, A. M. (2018). Phase change material based cooling of photovoltaic panel: A simplified numerical model for the optimization of the phase change material layer and general economic evaluation. *Journal of Cleaner Production*, *189*, 738–745. https://doi.org/10.1016/j.jclepro.2018.04.057

Bai, Q., & Bai, Y. (2014). Subsea Pipeline Design, Analysis, and Installation. In *Subsea Pipeline Design, Analysis, and Installation*. https://doi.org/10.1016/C2010-0-67706-6

Bhadbhade, N., Yilmaz, S., Zuberi, J. S., Eichhammer, W., & Patel, M. K. (2020). The evolution of energy efficiency in Switzerland in the period 2000–2016. *Energy*. https://doi.org/10.1016/j.energy.2019.116526

Bland, A., Khzouz, M., Statheros, T., & Gkanas, E. I. (2017). PCMs for residential building applications: A short review focused on disadvantages and proposals for future development. In *Buildings*. https://doi.org/10.3390/buildings7030078

Büyüközkan, G., Karabulut, Y., & Mukul, E. (2018). A novel renewable energy selection model for United Nations' sustainable development goals. *Energy*. https://doi.org/10.1016/j.energy.2018.08.215

Caliskan, H. (2017). Energy, exergy, environmental, enviroeconomic, exergoenvironmental (EXEN) and exergoenviroeconomic (EXENEC) analyses of solar collectors. In *Renewable and Sustainable Energy Reviews*. https://doi.org/10.1016/j.rser.2016.11.203

Celik, A. N. (2006). Present status of photovoltaic energy in Turkey and life cycle techno-economic analysis of a grid-connected photovoltaic-house. In *Renewable and Sustainable Energy Reviews*. https://doi.org/10.1016/j.rser.2004.09.007

CFE (Comision Federal de Electricidad). (2018). *Consulta tu tarifa*. 2017. https://app.cfe.mx/Aplicaciones/CCFE/Tarifas/TarifasCRECasa/Casa.aspx

Charles R., L. (2017a). *Optimum Tilt of Solar Panels*. https://www.solarpaneltilt.com/

Charles R., L. (2017b). *Optimum Tilt of Solar Panels*.

Coskun, C., Toygar, U., Sarpdag, O., & Oktay, Z. (2017). Sensitivity analysis of implicit correlations for photovoltaic module temperature: A review. In *Journal of Cleaner Production*. https://doi.org/10.1016/j.jclepro.2017.07.080

CRE. (n.d.). *Comision reguladora de Energía - permisos de Electricidad*. 2017. https://www.gob.mx/cre

da Silva, R. M., & Fernandes, J. L. M. (2010). Hybrid photovoltaic/thermal (PV/T) solar systems simulation with Simulink/Matlab. *Solar Energy*, *84*(12), 1985–1996. https://doi.org/10.1016/j.solener.2010.10.004

Data sheet RT25HC Rubitherm Technologies GmbH Imhoffweg 6 D-12307 Berlin E-Mail: info@rubitherm.com Internet: www.rubitherm.com. (2020). https://www.rubitherm.eu/media/products/datasheets/Techdata_-RT25HC_EN_05092018.PDF

Data sheet RT28HC Rubitherm Technologies GmbH Imhoffweg 6 D-12307 Berlin E-Mail: info@rubitherm.com Internet: www.rubitherm.com. (2020). https://www.rubitherm.eu/media/products/datasheets/Techdata_-RT28HC_EN_06082018.PDF

Data sheet RT35HC Rubitherm Technologies GmbH Imhoffweg 6 D-12307 Berlin E-Mail: info@rubitherm.com Internet: www.rubitherm.com. (2020). https://www.rubitherm.eu/media/products/datasheets/Techdata_-RT35HC_EN_06082018.PDF

Diallo, T. M. O., Yu, M., Zhou, J., Zhao, X., Shittu, S., Li, G., Ji, J., & Hardy, D. (2019). Energy performance analysis of a novel solar PVT loop heat pipe employing a microchannel heat pipe evaporator and a PCM triple heat exchanger. *Energy*. https://doi.org/10.1016/j.energy.2018.10.192

Dincer, I., Rosen, M. A., & Ahmadi, P. (2017). Optimization of energy systems. In *Optimization of Energy Systems*. https://doi.org/10.1002/9781118894484

Duffie, J. A., & Beckman, W. A. (2013). *Solar Engineering of Thermal Processes* (4th

Editio). John Wiley & Sons.

Electricity Sector Outlook 2017-2031, Secretaria de energia (SNER), Mexico. (2017). https://www.gob.mx/cms/uploads/attachment/file/325634/Electricity_Sector_Outlook_2017-2031.pdf

ESMAP, SOLARGIS, WB, & IFC. (2019). Global Solar Atlas. *Global Solar Atlas*.

Fayaz, H., Nasrin, R., Rahim, N. A., & Hasanuzzaman, M. (2018). Energy and exergy analysis of the PVT system: Effect of nanofluid flow rate. *Solar Energy*. https://doi.org/10.1016/j.solener.2018.05.004

Fayaz, H., Rahim, N. A., Hasanuzzaman, M., Nasrin, R., & Rivai, A. (2019). Numerical and experimental investigation of the effect of operating conditions on performance of PVT and PVT-PCM. *Renewable Energy*. https://doi.org/10.1016/j.renene.2019.05.041

Fayaz, H., Rahim, N. A., Hasanuzzaman, M., Rivai, A., & Nasrin, R. (2019). Numerical and outdoor real time experimental investigation of performance of PCM based PVT system. *Solar Energy*, *179*(July 2018), 135–150. https://doi.org/10.1016/j.solener.2018.12.057

Gaur, A., Ménézo, C., & Giroux-Julien, S. (2017). Numerical studies on thermal and electrical performance of a fully wetted absorber PVT collector with PCM as a storage medium. *Renewable Energy*. https://doi.org/10.1016/j.renene.2017.01.062

Greenspec. (2020). *Insulation materials and their thermal properties*. http://www.greenspec.co.uk/building-design/insulation-materials-thermal-properties/

Gu, Y., Zhang, X., Are Myhren, J., Han, M., Chen, X., & Yuan, Y. (2018). Techno-economic analysis of a solar photovoltaic/thermal (PV/T) concentrator for building application in Sweden using Monte Carlo method. *Energy Conversion and Management*, *165*(March), 8–24. https://doi.org/10.1016/j.enconman.2018.03.043

Hammami, M., Torretti, S., Grimaccia, F., & Grandi, G. (2017). Thermal and performance analysis of a photovoltaic module with an integrated energy storage system. *Applied Sciences (Switzerland)*. https://doi.org/10.3390/app7111107

Hazi, A., Hazi, G., Grigore, R., & Vernica, S. (2014). Opportunity to use PVT systems for water heating in industry. *Applied Thermal Engineering*, *63*(1), 151–157. https://doi.org/10.1016/j.applthermaleng.2013.11.010

Herrando, M., Pantaleo, A. M., Wang, K., & Markides, C. N. (2019). Solar combined cooling, heating and power systems based on hybrid PVT, PV or solar-thermal collectors for building applications. *Renewable Energy*, *143*, 637–647. https://doi.org/10.1016/j.renene.2019.05.004

Herrando, M., Ramos, A., Freeman, J., Zabalza, I., & Markides, C. N. (2018). Technoeconomic modelling and optimisation of solar combined heat and power systems based on flat-box PVT collectors for domestic applications. *Energy Conversion and Management*, *175*, 67–85.

https://doi.org/10.1016/j.enconman.2018.07.045

Hossain, M. S., Pandey, A. K., Selvaraj, J., Rahim, N. A., Islam, M. M., & Tyagi, V. V. (2018). Two side serpentine flow based photovoltaic-thermal-phase change materials (PVT-PCM) system: Energy, exergy and economic analysis. *Renewable Energy*. https://doi.org/10.1016/j.renene.2018.10.097

Hosseinzadeh, M., Sardarabadi, M., & Passandideh-Fard, M. (2018). Energy and exergy analysis of nanofluid based photovoltaic thermal system integrated with phase change material. *Energy*. https://doi.org/10.1016/j.energy.2018.01.073

INEGI. (2014). Instituto Nacional de Estadística y Geografía (México). In *Anuario estadístico y geográfico de los Estados Unidos Mexicanos 2014*.

Iv, J. H. L., & Lienhard, J. H. (1986). A heat transfer textbook. *Journal of Heat Transfer*. https://doi.org/10.1115/1.3246887

Jacobson, M. Z., & Jadhav, V. (2018). World estimates of PV optimal tilt angles and ratios of sunlight incident upon tilted and tracked PV panels relative to horizontal panels. *Solar Energy*, *169*, 55–66. https://doi.org/10.1016/j.solener.2018.04.030

Jahromi, S. N., Vadiee, A., & Yaghoubi, M. (2015). Exergy and Economic Evaluation of a Commercially Available PV/T Collector for Different Climates in Iran. *Energy Procedia*, *75*, 444–456. https://doi.org/10.1016/j.egypro.2015.07.416

Jesumathy, S. P., Udayakumar, M., & Suresh, S. (2012). Heat transfer characteristics in latent heat storage system using paraffin wax. *Journal of Mechanical Science and Technology*. https://doi.org/10.1007/s12206-011-1017-4

Jiménez-Xamán, C., Xamán, J., Moraga, N. O., Hernández-Pérez, I., Zavala-Guillén, I., Arce, J., & Jiménez, M. J. (2019). Solar chimneys with a phase change material for buildings: An overview using CFD and global energy balance. In *Energy and Buildings*. https://doi.org/10.1016/j.enbuild.2019.01.014

Jones, A. D., & Underwood, C. P. (2001). A thermal model for photovoltaic systems. *Solar Energy*, *4*, 349–359. https://doi.org/10.1016/S0038-092X(00)00149-3

Kalogirou, S. (2009). Solar Energy Engineering. In *Solar Energy Engineering*. https://doi.org/10.1016/B978-0-12-374501-9.X0001-5

Kant, K., Shukla, A., Sharma, A., & Biwole, P. H. (2016). Heat transfer studies of photovoltaic panel coupled with phase change material. *Solar Energy*. https://doi.org/10.1016/j.solener.2016.11.006

Kazem, H. A., Albadi, M. H., Al-Waeli, A. H. A., Al-Busaidi, A. H., & Chaichan, M. T. (2017). Techno-economic feasibility analysis of 1MW photovoltaic grid connected system in Oman. *Case Studies in Thermal Engineering*. https://doi.org/10.1016/j.csite.2017.05.008

Kazemian, A., Hosseinzadeh, M., Sardarabadi, M., & Passandideh-Fard, M. (2018). Experimental study of using both ethylene glycol and phase change material as coolant in photovoltaic thermal systems (PVT) from energy, exergy and entropy generation viewpoints. *Energy*. https://doi.org/10.1016/j.energy.2018.07.069

Khanna, S., Reddy, K. S., & Mallick, T. K. (2018a). Climatic behaviour of solar

photovoltaic integrated with phase change material. *Energy Conversion and Management*. https://doi.org/10.1016/j.enconman.2018.04.056

Khanna, S., Reddy, K. S., & Mallick, T. K. (2018b). Optimization of solar photovoltaic system integrated with phase change material. *Solar Energy*. https://doi.org/10.1016/j.solener.2018.01.002

Kim, J. H., Park, S. H., & Kim, J. T. (2014). Experimental performance of a photovoltaic-thermal air collector. *Energy Procedia*. https://doi.org/10.1016/j.egypro.2014.02.102

Kim, J. Y., Jeon, G. Y., & Hong, W. H. (2009). The performance and economical analysis of grid-connected photovoltaic systems in Daegu, Korea. *Applied Energy*. https://doi.org/10.1016/j.apenergy.2008.04.006

Kim, K. M., Moon, H., Park, J. S., & Cho, H. H. (2014). Optimal design of impinging jets in an impingement/effusion cooling system. *Energy*, *66*, 839–848. https://doi.org/10.1016/j.energy.2013.12.024

Klein, S. A. (2010). TRNSYS 17: A Transient System Simulation Program. *Solar Energy Laboratory, University of Wisconsin, Madison, USA*, *1*, 1–5. http://www.trnsys.com/

Kottek, M., Grieser, J., Beck, C., Rudolf, B., & Rubel, F. (2006). World map of the Köppen-Geiger climate classification updated. *Meteorologische Zeitschrift*. https://doi.org/10.1127/0941-2948/2006/0130

Lazard. (2018). Lazard's levelized cost of storage analysis — version 12.0. *Lazard's Levelized Cost of Storage - Version 12.0*.

Li, G., Pei, G., Ji, J., Yang, M., Su, Y., & Xu, N. (2015). Numerical and experimental study on a PV/T system with static miniature solar concentrator. *Solar Energy*, *120*, 565–574. https://doi.org/10.1016/j.solener.2015.07.046

Li, Z., Ma, T., Zhao, J., Song, A., & Cheng, Y. (2019). Experimental study and performance analysis on solar photovoltaic panel integrated with phase change material. *Energy*, *178*, 471–486. https://doi.org/10.1016/j.energy.2019.04.166

Lu, Z. H., & Yao, Q. (2007). Energy analysis of silicon solar cell modules based on an optical model for arbitrary layers. *Solar Energy*, *81*, 636–647. https://doi.org/10.1016/j.solener.2006.08.014

M., B. (2012). A comparative study of hybrid diesel solar PV-wind power systems in rural areas in the Sultanate of Oman. *International Journal of Sustainable Energy*, *31(2):95e1*(October 2012), 95e106.

Ma, T., Zhao, J., & Li, Z. (2018). Mathematical modelling and sensitivity analysis of solar photovoltaic panel integrated with phase change material. *Applied Energy*, *228*(July), 1147–1158. https://doi.org/10.1016/j.apenergy.2018.06.145

Maatallah, T., Zachariah, R., & Al-Amri, F. G. (2019). Exergo-economic analysis of a serpentine flow type water based photovoltaic thermal system with phase change material (PVT-PCM/water). *Solar Energy*, *193*(September), 195–204. https://doi.org/10.1016/j.solener.2019.09.063

Malvi, C. S., Dixon-Hardy, D. W., & Crook, R. (2011). Energy balance model of

combined photovoltaic solar-thermal system incorporating phase change material. *Solar Energy*. https://doi.org/10.1016/j.solener.2011.03.027

McAdams, W. H. (1954). Heat transmission. In *Industrial and Engineering Chemistry*. https://doi.org/10.1021/ie50031a003

Mengjie, S., Pun, W. M., Swapnil, D., Dongmei, P., & Ning, M. (2017). Thermal stability of organic binary PCMs for energy storage. *Energy Procedia*. https://doi.org/10.1016/j.egypro.2017.12.459

Milousi, M., Souliotis, M., Arampatzis, G., & Papaefthimiou, S. (2019). Evaluating the environmental performance of solar energy systems through a combined life cycle assessment and cost analysis. *Sustainability (Switzerland)*, *11*(9). https://doi.org/10.3390/su11092539

Modjinou, M., Ji, J., Yuan, W., Zhou, F., Holliday, S., Waqas, A., & Zhao, X. (2019). Performance comparison of encapsulated PCM PV/T, microchannel heat pipe PV/T and conventional PV/T systems. *Energy*, *166*(November), 1249–1266. https://doi.org/10.1016/j.energy.2018.10.007

Mohammadi, K., Naderi, M., & Saghafifar, M. (2018). Economic feasibility of developing grid-connected photovoltaic plants in the southern coast of Iran. *Energy*. https://doi.org/10.1016/j.energy.2018.05.065

Mondal, A. H., & Denich, M. (2010). Hybrid systems for decentralized power generation in Bangladesh. *Energy for Sustainable Development*. https://doi.org/10.1016/j.esd.2010.01.001

Nižetić, S., Arıcı, M., Bilgin, F., & Grubišić-Čabo, F. (2018). Investigation of pork fat as potential novel phase change material for passive cooling applications in photovoltaics. *Journal of Cleaner Production*. https://doi.org/10.1016/j.jclepro.2017.09.164

PerfectHome Solar Panels. (2020). https://perfecthome.mx/

Petela, R. (2003). Exergy of undiluted thermal radiation. *Solar Energy*. https://doi.org/10.1016/S0038-092X(03)00226-3

Petela, R. (2008). An approach to the exergy analysis of photosynthesis. *Solar Energy*. https://doi.org/10.1016/j.solener.2007.09.002

Piacentino, A., Duic, N., Markovska, N., Mathiesen, B. V., Guzović, Z., Eveloy, V., & Lund, H. (2019). Sustainable and cost-efficient energy supply and utilisation through innovative concepts and technologies at regional, urban and single-user scales. In *Energy*. https://doi.org/10.1016/j.energy.2019.06.015

Pidwinry, M. (2011). Köppen Climate Classification System. *Encyclopedia of Earth*, 1–8. https://doi.org/10.5194/hess-11-1633-2007

Preet, S., Bhushan, B., & Mahajan, T. (2017). Experimental investigation of water based photovoltaic/thermal (PV/T) system with and without phase change material (PCM). *Solar Energy*, *155*, 1104–1120. https://doi.org/10.1016/j.solener.2017.07.040

Qiu, Z., Zhao, X., Li, P., Zhang, X., Ali, S., & Tan, J. (2015). Theoretical investigation of

the energy performance of a novel MPCM (Microencapsulated Phase Change Material) slurry based PV/T module. *Energy*, *87*, 686–698. https://doi.org/10.1016/j.energy.2015.05.040

Raman, V., & Tiwari, G. N. (2008). Life cycle cost analysis of HPVT air collector under different Indian climatic conditions. *Energy Policy*, *36*(2), 603–611. https://doi.org/10.1016/j.enpol.2007.08.031

Ren, X., Yu, M., Zhao, X., Li, J., Zheng, S., Chen, F., Wang, Z., Zhou, J., Pei, G., & Ji, J. (2020). Assessment of the cost reduction potential of a novel loop-heat-pipe solar photovoltaic/thermal system by employing the distributed parameter model. *Energy*, *190*, 116338. https://doi.org/10.1016/j.energy.2019.116338

Rounis, E. D., Athienitis, A. K., & Stathopoulos, T. (2016). Multiple-inlet Building Integrated Photovoltaic/Thermal system modelling under varying wind and temperature conditions. *Solar Energy*, *139*, 157–170. https://doi.org/10.1016/j.solener.2016.09.023

Santika, W. G., Anisuzzaman, M., Simsek, Y., Bahri, P. A., Shafiullah, G. M., & Urmee, T. (2020). Implications of the Sustainable Development Goals on national energy demand: The case of Indonesia. *Energy*, *196*. https://doi.org/10.1016/j.energy.2020.117100

Sardarabadi, M., Passandideh-Fard, M., Maghrebi, M. J., & Ghazikhani, M. (2017). Experimental study of using both ZnO/ water nanofluid and phase change material (PCM) in photovoltaic thermal systems. *Solar Energy Materials and Solar Cells*, *161*(June 2016), 62–69. https://doi.org/10.1016/j.solmat.2016.11.032

Shan, F., Cao, L., & Fang, G. (2013). Dynamic performances modeling of a photovoltaic-thermal collector with water heating in buildings. *Energy and Buildings*. https://doi.org/10.1016/j.enbuild.2013.07.067

Shan, F., Tang, F., Cao, L., & Fang, G. (2014). Comparative simulation analyses on dynamic performances of photovoltaic-thermal solar collectors with different configurations. *Energy Conversion and Management*. https://doi.org/10.1016/j.enconman.2014.07.077

Singh, P., Khanna, S., Becerra, V., Newar, S., Sharma, V., Mallick, T. K., Hutchinson, D., Radulovic, J., & Khusainov, R. (2020). Power improvement of finned solar photovoltaic phase change material system. *Energy*, *193*, 116735. https://doi.org/10.1016/j.energy.2019.116735

Skoplaki, E., & Palyvos, J. A. (2009). On the temperature dependence of photovoltaic module electrical performance: A review of efficiency/power correlations. *Solar Energy*. https://doi.org/10.1016/j.solener.2008.10.008

Smith, C. J., Forster, P. M., & Crook, R. (2014). Global analysis of photovoltaic energy output enhanced by phase change material cooling. *Applied Energy*, *126*, 21–28. https://doi.org/10.1016/j.apenergy.2014.03.083

Sohani, A., Farasati, Y., & Sayyaadi, H. (2017). A systematic approach to find the best road map for enhancement of a power plant with dew point inlet air pre-cooling of the air compressor. *Energy Conversion and Management*, *150*(August), 463–484.

https://doi.org/10.1016/j.enconman.2017.08.028

Sohani, A., & Sayyaadi, H. (2020). End-users' and policymakers' impacts on optimal characteristics of a dew-point cooler. *Applied Thermal Engineering*, *165*. https://doi.org/10.1016/j.applthermaleng.2019.114575

Sohani, A., Sayyaadi, H., & Mohammadhosseini, N. (2018). Comparative study of the conventional types of heat and mass exchangers to achieve the best design of dew point evaporative coolers at diverse climatic conditions. *Energy Conversion and Management*. https://doi.org/10.1016/j.enconman.2017.12.042

Stropnik, R., & Stritih, U. (2016). Increasing the efficiency of PV panel with the use of PCM. *Renewable Energy*, *97*, 671–679. https://doi.org/10.1016/j.renene.2016.06.011

Su, D., Jia, Y., Alva, G., Liu, L., & Fang, G. (2017). Comparative analyses on dynamic performances of photovoltaic–thermal solar collectors integrated with phase change materials. *Energy Conversion and Management*, *131*, 79–89. https://doi.org/10.1016/j.enconman.2016.11.002

Su, D., Jia, Y., Lin, Y., & Fang, G. (2017). Maximizing the energy output of a photovoltaic–thermal solar collector incorporating phase change materials. *Energy and Buildings*, *153*, 382–391. https://doi.org/10.1016/j.enbuild.2017.08.027

Tariq, R., Zhan, C., Zhao, X., & Sheikh, N. A. (2018). Numerical study of a regenerative counter flow evaporative cooler using alumina nanoparticles in wet channel. *Energy and Buildings*, *169*(169), 430–443. https://doi.org/10.1016/j.enbuild.2018.03.086

Tariq, Rasikh, & Sheikh, N. A. (2018). Numerical heat transfer analysis of Maisotsenko Humid Air Bottoming Cycle – A study towards the optimization of the air-water mixture at bottoming turbine inlet. *Applied Thermal Engineering*, *133*(March), 49–60. https://doi.org/10.1016/j.applthermaleng.2018.01.024

Tariq, Rasikh, Sheikh, N. A., Xamán, J., & Bassam, A. (2018). An innovative air saturator for humidification-dehumidification desalination application. *Applied Energy*, *228*(July), 789–807. https://doi.org/10.1016/j.apenergy.2018.06.135

Tariq, Rasikh, Sheikh, N. A., Xamán, J., & Bassam, A. (2019). Recovering waste energy in an indirect evaporative cooler – A case for combined space air conditioning for human occupants and produce commodities. *Building and Environment*, *152*(November 2018), 105–121. https://doi.org/10.1016/j.buildenv.2019.01.038

Thermtest instruments, MATERIALS THERMAL PROPERTIES DATABASE. (2020a). https://thermtest.com/materials-database

Thermtest instruments, MATERIALS THERMAL PROPERTIES DATABASE. (2020b).

Tiwari, A., & Sodha, M. S. (2006). Performance evaluation of solar PV/T system: An experimental validation. *Solar Energy*, *80*(7), 751–759. https://doi.org/10.1016/j.solener.2005.07.006

Tiwari, S., Agrawal, S., & Tiwari, G. N. (2018). PVT air collector integrated greenhouse

dryers. In *Renewable and Sustainable Energy Reviews*. https://doi.org/10.1016/j.rser.2018.03.043

Tripathy, M., Joshi, H., & Panda, S. K. (2017). Energy payback time and life-cycle cost analysis of building integrated photovoltaic thermal system influenced by adverse effect of shadow. *Applied Energy*, *208*, 376–389. https://doi.org/10.1016/j.apenergy.2017.10.025

Wajs, J., Golabek, A., Bochniak, R., & Mikielewicz, D. (2020). Air-cooled photovoltaic roof tile as an example of the BIPVT system e An experimental study on the energy and exergy performance. *Energy*, *197*, 117255. https://doi.org/10.1016/j.energy.2020.117255

Wang, K., Herrando, M., Pantaleo, A. M., & Markides, C. N. (2019). Technoeconomic assessments of hybrid photovoltaic-thermal vs. conventional solar-energy systems: Case studies in heat and power provision to sports centres. *Applied Energy*. https://doi.org/10.1016/j.apenergy.2019.113657

Yazdanifard, F., Ebrahimnia-Bajestan, E., & Ameri, M. (2016). Investigating the performance of a water-based photovoltaic/thermal (PV/T) collector in laminar and turbulent flow regime. *Renewable Energy*, *99*, 295–306. https://doi.org/10.1016/j.renene.2016.07.004

Yuan, W., Ji, J., Modjinou, M., Zhou, F., Li, Z., Song, Z., Huang, S., & Zhao, X. (2018). Numerical simulation and experimental validation of the solar photovoltaic/thermal system with phase change material. *Applied Energy*, *232*(July), 715–727. https://doi.org/10.1016/j.apenergy.2018.09.096

Zhao, J., Ma, T., Li, Z., & Song, A. (2019). Year-round performance analysis of a photovoltaic panel coupled with phase change material. *Applied Energy*. https://doi.org/10.1016/j.apenergy.2019.04.004